Acta Materialia 255 (2023) 119074

Contents lists available at ScienceDirect

Acta Materialia

journal homepage: www.elsevier.com/locate/actamat

Full length article

Theoretical and experimental grain boundary energies in body-centered cubic metals

Changle Li [a], Song Lu [a,*], Sergiy Divinski [b], Levente Vitos [a,c,d]

[a] Applied Materials Physics, Department of Materials Science and Engineering, KTH Royal Institute of Technology, SE-10044 Stockholm, Sweden
[b] Institute of Materials Physics, University of Münster, Münster 48149, Germany
[c] Department of Physics and Astronomy, Division of Materials Theory, Uppsala University, Box 516, SE-75120 Uppsala, Sweden
[d] Research Institute for Solid State Physics and Optics, Wigner Research Center for Physics, P.O. Box 49, H-1525 Budapest, Hungary

ARTICLE INFO

Keywords:
Grain boundary energy
Temperature dependence
Surface energy
Ab initio
Bcc metals

ABSTRACT

Grain boundary energy (GBE) and its temperature dependence in body-centered cubic (bcc) metals are investigated using *ab initio* calculations. We reveal a scaling relationship between the GBEs of the same grain boundary structure in different bcc metals and find that the scaling factor can be best estimated by the ratio of the low-index surface energy. Applying the scaling relationship, the general GBEs of bcc metals at 0 K are predicted. Furthermore, adopting the Foiles's method which assumes that the general GBE has the same temperature dependence as the elastic modulus c_{44} [Scr. Mater., 62 (2010) 231–234], the predicted general GBEs at elevated temperatures are found in good agreement with available experimental data. Reviewing two experimental methods for determining the general GBEs, we conclude that the two sets of experimental GBEs for bcc metals correspond to different GB structural spaces and differ by approximately a factor of 2. The present work puts forward an efficient methodology for predicting the general GBEs of metals, which has the potential to extend its application for homogeneous alloys without strong segregation of the alloying element and facilitates GB engineering for advanced alloy design.

1. Introduction

During the last decades, tailoring the properties of grain boundaries (GBs) by controlling alloying segregation/depletion and GB character distribution, often referred to as 'grain boundary engineering' [1,2], has been developed as an important strategy for improving the mechanical properties of alloys. The atomic structures and energetics of GBs are intimately related to various physical and mechanical properties including plasticity, corrosion resistance, conductivity, and so on [3]. Particularly, the grain boundary energy (GBE, γ_{gb}) is a key parameter in studying processes such as segregation, precipitation, diffusion, and cracking, etc. [4,5].

Extensive experimental efforts have been devoted to determining the GBEs, and two intrinsically indirect methods were often used. One such experimental approach, the *thermal grooving method (T.G.)*, determines the relative GBEs by measuring the angles of the equilibrium thermal grooves at GB-surface triple junctions [6,7], as adopted in the zero-creep and multiphase equilibrium techniques [8–10]. This method requires knowledge of the free surface energy (FSE, γ_{fs}) to translate the measured relative γ_{gb}/γ_{fs} ratio to the absolute GBE. Unfortunately, the accurate determination of the FSEs by experiments is as challenging as for the GBEs. The thermal grooving method has been applied to determine the general GBEs in various face-centered cubic (fcc) metals [8,9,11–14] and alloys [11,13,15], as well as in bcc metals [16–20]. The same approach can also be used to study the orientation dependence of the GBE for specific symmetrical tilt [21,22] and twist [23] GBs at high temperatures. The results may be strongly affected by anisotropy of the surface energy [24,25], surface faceting [26], GB motion during annealing treatment [27,28], etc. Nevertheless, a reliable spectrum of relative GBEs can be safely determined revealing, e.g., significant modifications of the interface energies via external stimuli, such as plastic deformation [29,30].

Another commonly adopted, in fact semi-empirical method for estimating the GBE is the *GB diffusion approach (Diff.)*, which determines the GBE through a relationship between the measured GB and lattice self-diffusivities [31–34]. The model was originally proposed by Borisov [31] and elaborated later by Guiraldenq [32] and Gupta [33]. According to this approach, the GBE is estimated by the decrease in the activation energy for GB diffusion compared to that for lattice diffusion.

In a previous study [35], Pelleg examined the GBEs for fcc metals (Ag, Ni, γ-Fe) obtained from the above T.G. and Diff. approaches and

* Corresponding author.
E-mail address: songlu@kth.se (S. Lu).

https://doi.org/10.1016/j.actamat.2023.119074
Received 6 February 2023; Received in revised form 10 May 2023; Accepted 5 June 2023
Available online 8 June 2023

concluded that a good agreement can be generally reached. Gupta [33,36] showed that the GBE and its temperature dependence for Au and Au–Ta alloys can be satisfyingly obtained from the GB and lattice self-diffusion data; as a by-product, one may estimate the segregation energy of a solute. Recently, the GBE of Ni has been determined by Haremski et al. [37] using the thermal grooving method and by Divinski et al. [38] using the diffusivity data, and an agreement between the two sets of data was reached. Extensions of the Diff. method towards the determination of the GBEs in alloys, including multi-component ones, were recently discussed, too [39,40]. However, for metals with the bcc structure (e.g., α-Fe), the agreement between the two methods was found worse. Difficulties also arise when applying Diff. method to hexagonal close-packed (hcp) metals, in which it is not trivial to define an effective density of GB atoms from the lattice parameters.

Despite that experimental techniques for determining GBEs exist, the obtained values are usually widely scattered, and it is still cumbersome to conduct these experiments in alloys. Typically, the general GBEs in alloys, as well as the composition and temperature dependence, are not available. Alternatively, one can explore the use of atomistic simulations, such as the empirical potentials and density functional theory (DFT) calculations, to investigate GBs. GB studies for pure metals using the embedded atom method (EAM) have led to a better understanding of the atomic structures and their energetics. For example, Holm et al. [41–43] calculated numerous GBEs in pure metals and found a strong correlation between GBEs of the same crystallographical type in different materials. In comparison to atomistic studies using empirical potentials, DFT calculations are usually more accurate and have better predictive power. However, due to the extensive computational cost, DFT calculations are usually limited to pure metals or simple dilute alloys for low-index coincidence site lattice (CSL) types of GBs. Zheng et al. [44] recently developed a database of GBEs using high-throughput *ab initio* calculations, which includes ten types of low-index GBEs for 58 elemental metals. It is important to note that DFT GBEs are usually obtained at 0 K, and proper approximations for the temperature effect should be considered when compared to the high-temperature experimental values. The comparison is further impeded by the fact that DFT simulations and experiments are usually done for special and general GBs, respectively.

Theoretical study about the temperature dependence of GBE is rare. Due to the large variety of GB structures, it is a challenging task to compute the phonon contribution to the temperature-dependent GBE using DFT calculations. A few attempts are available in literature. For instance, Scheiber et al. [45] evaluated the temperature dependence of GBE for several low Σ index GBs in W using the quasiharmonic approximation with explicit phonon calculations. The obtained GBEs showed a monotonous decrease with increasing temperature. Besides, there are also attempts to describe the temperature dependence of GBE through materials' intrinsic parameters like elastic constants, shear moduli, and cohesive energy. Foiles [46] compared the temperature dependence of a general GBE and shear moduli from empirical potential calculations and found that the GBE and shear modulus share approximately the same temperature dependence up to about $0.75T_m$ (T_m, the melting temperature). Scheiber et al. assessed this method by comparing to their DFT GBEs for W, and they showed that the Foiles's method works very well up to approximately 0.55 T_m for GBs with different Σ values. Cheng et al. [47] explored an alternative model to predict the temperature dependence of GBE via the temperature-dependent specific heat. However, according to Scheiber [45], it can only provide a qualitative trend. In addition to the numerical calculations with different crystallographic structures, recent studies have introduced mathematical models to predict GBEs, as demonstrated by Runnels et al. [48–50]. They introduced a bond matching model to predict anisotropic GBEs with tilt and twist grain boundaries and extended it to both fcc and bcc materials. The scalability of this model across different metals allows for universal application, and its performance has been shown to agree strongly with available EAM data.

Table 1
The structural properties of the studied [1$\bar{1}$0] tilt GBs. In the last column we give the number of atoms within the supercell used to model the corresponding GBs.

Index	Angle	GB-plane	Number of atoms
Σ3	109.47°	(1 1 1)	30
Σ3	70.53°	(1 1 2)	24
Σ9	38.94°	(1 1 4)	34
Σ9	141.06°	(2 2 1)	68
Σ11	50.48°	(1 1 3)	66
Σ11	129.52°	(3 3 2)	42
Σ17	86.63°	(2 2 3)	64
Σ17	93.37°	(3 3 4)	66
Σ19	26.53°	(1 1 6)	72
Σ19	153.35°	(3 3 1)	70

The purpose of this work is to establish a feasible and yet robust *ab initio* based method for quickly predicting the GBEs in bcc metals. We start by calculating the GBEs at 0 K for seven bcc metals (V, Cr, Fe, Nb, Mo, Ta, and W) using first-principles calculations. Calculations for all selected metals are performed for 10 types of tilt symmetric GB structures, including one twin boundary and nine GBs with high misorientation angles. Analyzing the obtained results shows that the GBEs of the same GB structure in a pair of bcc metals are scaled by a materials-dependent parameter δ_{gb}. The scaling parameters δ, particularly δ_{gb} for GBs introduced in the present work, have not to be mixed with the GB width often denoted in the literature using a similar symbol. We compare the averaged ratio of GBEs with those derived from other physical parameters, including the ratios of free surface energy (δ_{fs}), elastic constant ($\delta_{a_0c_{44}}$), shear modulus ($\delta_{a_0G_V}$), and cohesive energy (δ_{E_{coh}/a_0^2}), and find that the scaling prefactor (δ_{gb}) is best estimated by the ratio of the low-index surface energy. The same scaling relationship is expected for the general GBEs from experiments, which are discussed in detail. Surprisingly, we observe that the two sets of experimental GBEs from the above-mentioned experimental methods (T.G. and Diff.) differ by approximately a factor of 2, for which we present a throughout discussion to understand the reason. Furthermore, using the scaling relationship, we first predict the 0 K general GBEs for various metals and then extrapolate the 0 K GBEs to elevated temperatures by assessing the temperature dependence of the shear modulus. The proposed approach yields GBEs at elevated temperatures in reasonable agreement with the available experimental data. Finally, we apply our method to predict the general GBEs of Fe–Cr solid solutions and discuss the limitations when applying the scaling method for predicting GBEs in alloys without considering GB segregation. Thus, the current methodology is proposed for the case of a non-segregating alloying element.

2. Methodology

2.1. GB properties

Ten symmetric tilt GBs with the [1$\bar{1}$0] tilt axis are studied and listed in Table 1. All the GBs are initiated from the tilt plane with certain misorientation angles. The schematic of the atomic structures of the studied GBs is presented in Fig. S1 in Supplementary Material (SM).

The GBE (γ_{gb}, in units of J/m^2) is defined as

$$\gamma_{gb} = \frac{E_{gb}^{sc} - N_{gb}E_b}{2A_{gb}}, \quad (1)$$

where E_{gb}^{sc} is the total energy of the supercell with two identical GBs, N_{gb} is the number of atoms in the supercell (Table 1), E_b is the reference bulk energy (per atom) calculated from a bcc primitive cell, A_{gb} is the area of the GB. The factor of 2 stands for the two GBs in the supercell. We notice that in literature the reference bulk energy may be obtained in different ways, for example using a GB-free supercell of the same size as that for the GB (in order to minimize the error due to the

calculation parameters like the k-point mesh) or using the incremental method [51], which can result in slightly different GBEs. We have compared our obtained GBEs with available data in the literature and found good agreement (Section 3.1). Furthermore, considering that the GBEs are obtained in consistent manner, our main findings and conclusions are not affected.

2.2. Free surface, cohesive, and elastic properties

For the purpose to analyze the relationship between the GBEs and other materials properties, the free surface energies, cohesive energy, and elastic properties are also calculated. Specifically, the free surface energy ($\gamma_{\rm fs}$, in units of J/m^2) is calculated by

$$\gamma_{\rm fs} = \frac{E_{\rm fs}^{sc} - N_{\rm fs}E_{\rm b}}{2A_{\rm fs}}, \tag{2}$$

where $E_{\rm fs}^{sc}$ is the total energy of the supercell with two free surfaces, $N_{\rm fs}$ is the number of atoms in the surface structure, $A_{\rm fs}$ is the area of the surface. The cohesive energy ($E_{\rm coh}$, in units of eV/atom) is expressed as

$$E_{\rm coh} = E_{\rm b} - E_{\rm iso}, \tag{3}$$

where $E_{\rm iso}$ is the total energy of an isolated atom.

For a cubic structure, there are three independent single-crystal elastic constants, c_{11}, c_{12}, and c_{44}. Usually, the elastic constants at the equilibrium volumes are calculated using an efficient stress–strain energy method [52]. A set of strains ($e = e_1, e_2, e_3, e_4, e_5, e_6$) is used to generate the small distortions of unit cell. The corresponding stresses ($s = s_1, s_2, s_3, s_4, s_5, s_6$) caused by the applied strains are obtained from first-principles calculations for the deformed crystals. More details are described in Ref. [52]. The polycrystalline elastic constants, e.g., bulk modulus (B) and shear modulus (G), are calculated by the Voigt–Reuss–Hill approach.

2.3. Computational details

All DFT calculations are performed using the Vienna *ab initio* simulations package (VASP) [53] and the projector augmented-wave (PAW) approach [54]. For the exchange–correlation (xc) functional we adopt the generalized gradient approximation (GGA) parameterized by the revised Perdew, Burke, and Ernzerhof functional for solids (PBEsol) [55]. The PAW potentials treat the p semi-core electrons as valence electrons, which means 11 valence electrons for V, Nb, and Ta, 12 valence electrons for Cr, Mo, and W, and 14 valence electrons for Fe. It is noted that including the semi-core p electrons as the valence electrons is important for accurate calculation of the surface energy for bcc metals [56,57]. Cutoff energies are set to 500 eV for all the calculations. For GB calculations, a careful $\boldsymbol{k}$-point test for each GB is done for bcc W (see SM Fig. S2), and the $\boldsymbol{k}$-point convergence criteria is set to an error in the GB energy of 0.02 J/m^2. The same set of $\boldsymbol{k}$-meshes is then adopted for other metals. Full geometry relaxation is performed and the convergence criteria for electronic energy and force calculations are 10^{-5} eV and 0.02 eV/Å, respectively. For free surface calculations, the $\boldsymbol{k}$-point convergence test for (100) and (110) planes are also carried out and the convergence criteria is kept the same as that for GB calculations. For cohesive energy calculation, the isolated atom is placed in a 15 × 15 × 15 Å cell, and the $\boldsymbol{k}$-point mesh is set to 3 × 3 × 3. For magnetic elements, Fe is treated as ferromagnetic (FM), whereas the antiferromagnetic (AFM) Cr is treated as nonmagnetic (NM).

3. Results

3.1. GBEs for bcc metals

In Fig. 1, we present the calculated $\gamma_{\rm gb}$ for (a) Fe, (b) Mo, and (c) W as a function of the [1$\bar{1}$0] tilt angle θ, in comparison with the previous DFT values [56] as well as the EAM results [56]. The comparison between the present ($\gamma_{\rm gb}^{\rm Pres.}$) and previous ($\gamma_{\rm gb}^{\rm Ref.}$) DFT results for these three metals and for the ten GBs is also presented in Fig. 1d. The energies of the [1$\bar{1}$0] symmetric tilt GBs in bcc Fe, Mo, and W metals exhibit a similar shape as a function of the tilt angle. There is a deep cusp located at the coherent twin boundary $\Sigma3(112)$ ($\theta = 70.53°$) and a shallow cusp at the $\Sigma11(332)$ ($\theta = 129.52°$) GB. Fig. 1d shows that the present calculated GBEs have an excellent agreement with the former DFT values, with $R^2 \approx 1.00$ and a standard error of ~ 0.005 J/m^2. The previous EAM γ-surfaces show a similar shape, and their GBEs for W agree well with the DFT results, but the absolute values for Fe and Mo are remarkably underestimated.

Fig. 2 compares the GB energies for all bcc metals considered here. The numerical values for all the studied bcc metals are listed in Table S1 in SM, where we also included the available DFT values for comparison. We observe that Group VI metals have high $\gamma_{\rm gb}$ while Group V metals have relatively low $\gamma_{\rm gb}$. Specifically, $\gamma_{\rm gb}$ of Fe in Group VIII is intermediate between those of Group V and Group VI metals. For Group VI metals, the highest values of $\gamma_{\rm gb}$ are found for W, followed by Cr and Mo, respectively. The calculated GBEs for Group V metals exhibit a similar ordering, viz., $\gamma_{\rm gb}^{\rm Ta} \geqslant \gamma_{\rm gb}^{\rm V} \geqslant \gamma_{\rm gb}^{\rm Nb}$. We conclude that in the same group, 5d metals have the highest values of $\gamma_{\rm gb}$, followed by 3d and then 4d metals.

3.2. Correlation between the GBEs in different bcc metals

In the following we analyze the correlations between the GBEs of the same GB structure in different bcc metals. Tungsten is taken as the reference and the pairwise comparisons are presented in Fig. 3. Previous DFT GBEs for twist and tilt GBs [44,56] are also presented in the figure when available. For a pair of metals, all the data points locate approximately on a straight line passing through the origin (as indicated by the dashed lines in Fig. 3). When fitted with a linear function, the mean absolute error (MAE) and the root mean square error (RMSE) for most of the studied metals are less than 0.1 J/m^2, which implies a strong correlation among the GBEs of the same structure. The slopes ($\delta_{\rm gb(fit)}^{M/W}$) from the linear fittings for the six pairs of metals are listed in Table 2, together with the MAE and RMSE values. Similar observations were reported by Ratanaphan et al. [43] using the embedded atom method (EAM) in Mo and Fe for 400 GBs. Although the EAM GBEs were strongly underestimated in comparison to the DFT results, a strong linear correlation among the GBEs in the two metals was still revealed. Similar correlations were also reported in fcc metals by EAM [41,43] and DFT calculations [56,58].

Notably, in fcc metals, our recent study showed that the correlation slope between the GBEs of a pair of metals is very close to the ratio of the (111) surface energies [58], with a deviation usually less than ~10%. In Fig. 3, the calculated FSEs for two low-index surfaces (100) and (110) in different metals are presented. The numerical values of the FSE ratios ($\delta_{\rm fs}^{M/W} \equiv \gamma_{\rm fs}^{M}/\gamma_{\rm fs}^{W}$) for the (100) and (110) surfaces are listed in Table 2, the $\delta_{\rm fs(100)}^{M/W}$ values are observed to be closer to $\delta_{\rm gb(fit)}^{M/W}$ than the $\delta_{\rm fs(110)}^{M/W}$ values. The deviations are the largest for V (28%) and Nb (23%), and relatively small (<10%) for other studied metals. Both ratios of the (100) and (110) FSEs are larger than $\delta_{\rm gb(fit)}$. A clear comparison among them is shown in Fig. 4a.

In literature, the scaling of the GBEs is usually related to physical parameters including the ratios of elastic constants (a_0c_{44}), shear modulus ($a_0G_{\rm V}$), cohesive energy ($E_{\rm coh}/a_0^2$), and twin boundary energy ($\gamma_{\rm tw}$). Using EAM calculations, Holm et al. [41] reported that the ratios of shear modulus a_0c_{44} and the Voigt average shear modulus

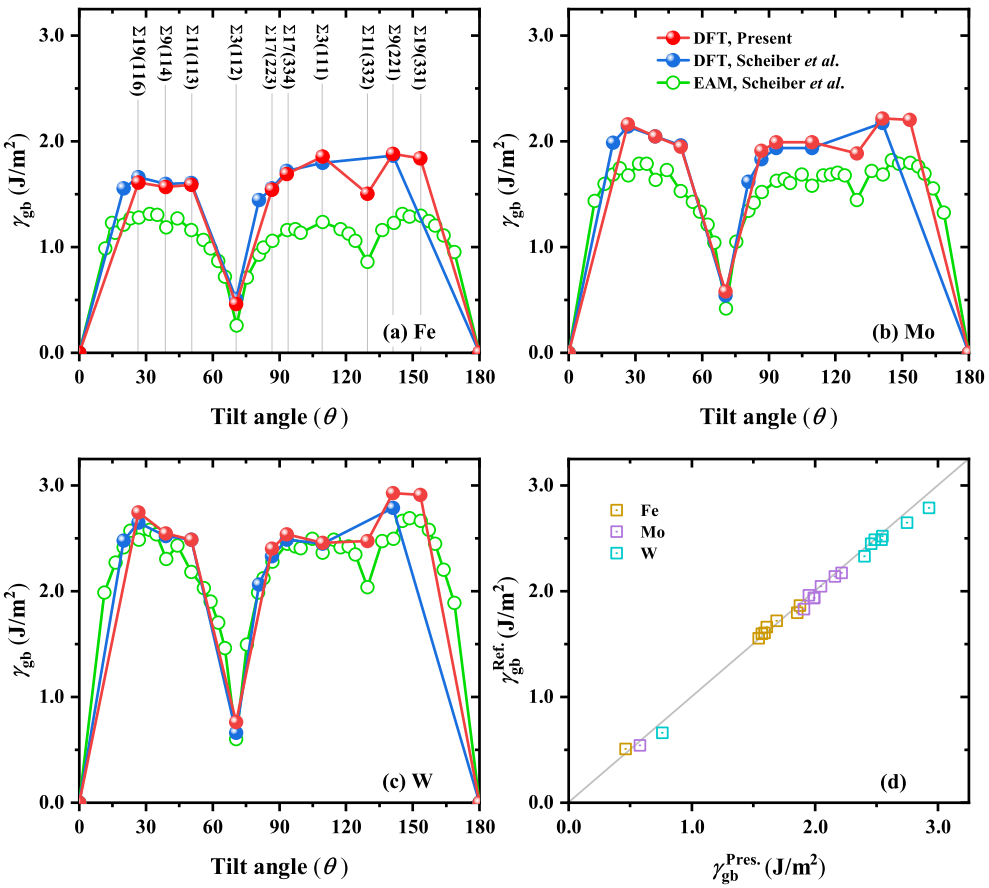

Fig. 1. Comparison of the calculated GBEs (γ_{gb}) between EAM (open symbols) and DFT (solid symbols) results for (a) Fe, (b) Mo, and (c) W as a function of the tilt angle (θ). Figure (d) presents the comparison between the present ($\gamma_{gb}^{Pres.}$) and previous ($\gamma_{gb}^{Ref.}$) [56] GBEs obtained by DFT calculations using the PBEsol exchange–correlation functionals.

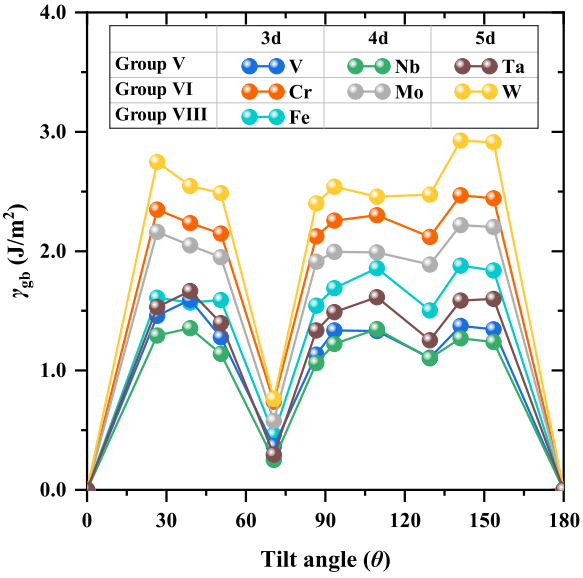

Fig. 2. The calculated γ_{gb} as a function of tilt angle (θ) for bcc metals.

a_0G_V are the closest parameters to estimate the slopes of the GBEs in selected fcc metals (Ni, Al, Au and Cu). However, in our recent DFT studies for ten fcc metals [58], we showed that the two ratios of moduli may strongly deviate from the actual scaling relations of the GBEs in some other fcc metals, e.g., by more than 20% in Co, Rh, and Ir. The ratio of the twin boundary energy in fcc metals deviates quite strongly from $\delta_{gb(fit)}$ for other GBs [58]. While in bcc metals, Ratanaphan et al. [43] showed that the scaling of the GBEs in Fe and Mo obtained by EAM calculations is best estimated by the ratio of the cohesive energies, and worstly represented by the ratios of the shear moduli. In order to identify the best physical parameters that may correlate with the scaling factors of the GBEs for most metals, in Fig. 4 we also compare $\delta^{M/W}_{E_{coh}/a_0^2}$, $\delta^{M/W}_{a_0G_V}$, $\delta^{M/W}_{a_0c_{44}}$ with the actual slopes $\delta^{M/W}_{gb(fit)}$ using data from both DFT calculations and experiments. The corresponding numerical values are found in Table 2 as well. For all the studied metals, $\delta^{M/W}_{fs}$ values are consistently closer to $\delta^{M/W}_{gb(fit)}$ compared to $\delta^{M/W}_{E_{coh}/a_0^2}$, $\delta^{M/W}_{a_0G_V}$, and $\delta^{M/W}_{a_0c_{44}}$, particularly for the ratio of the (100) FSE. This is also the case for fcc metals [58]. The ratio of the cohesive energy is close to the actual scaling factor only for Mo but deviates quite strongly for most of the studied metals. Among the three ratios of $\delta^{M/W}_{a_0c_{44}}$, $\delta^{M/W}_{a_0G_V}$, and $\delta^{M/W}_{E_{coh}/a_0^2}$, $\delta^{M/W}_{a_0G_V}$ is more likely to give a good estimation of the actual scaling factor for all the studied bcc metals. However, EAM results (Fig. 4b half solid symbols) show a different trend, which is ascribed to the low accuracy of the obtained quantities. We also observe that the $\Sigma3(112)$ twin boundary energies in bcc metals locate on the same line as other GBEs, in Fig. 3. This is different for the coherent $\Sigma3(111)$ twin boundary energy in fcc metals [58]. The ratios of $\Sigma3(112)$ twin boundary energy in bcc metals ($\delta^{M/W}_{tw}$) are listed in Table 3. Interestingly, these values are also very close to $\delta^{M/W}_{gb}$, although systematically underestimated, except Cr which is mainly due to its slight overestimation of the nonmagnetic GBEs. Based on the above observations, one can almost perfectly estimate $\delta_{gb(fit)}$ by averaging δ_{tw} and $\delta_{fs(100)}$. A possible explanation could be that γ_{fs} and γ_{tw} represent the upper and lower limits for the GBEs, respectively, and thus their average gives the closest mean slope for the GBEs.

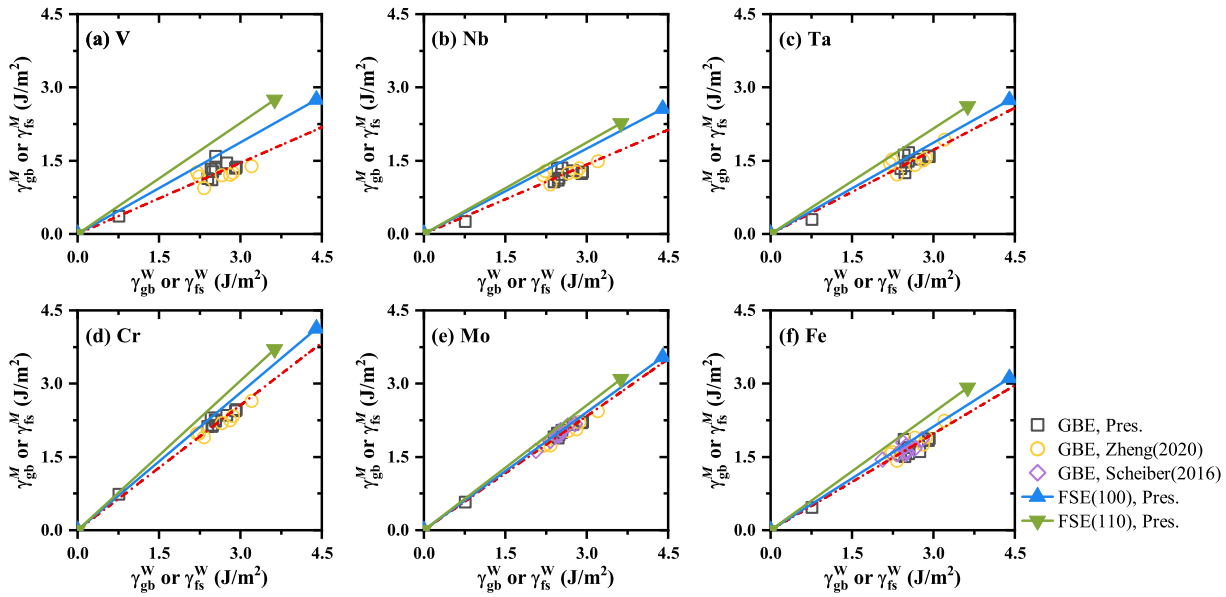

Fig. 3. Pairwise comparisons of the calculated GBEs, (100) and (110) FSEs for the studied metals taking W as the reference metal. The dash-dotted lines are the linear fittings to the GBEs including the present results (squares) and the previous DFT GBEs (circles and diamonds) for both tilt and twist GBs from Refs. [44,56].

Table 2
Surface energies for the (100) and (110) facets ($\gamma_{fs(100)}$ and $\gamma_{fs(110)}$, respectively, in units of J/m^2) and their ratios relative to that of W for the studied bcc metals. The ratios of E_{coh}/a_0^2, a_0G_V, a_0c_{44}, with the slopes ($\delta_{gb(fit)}^{M/W}$) from the linear fittings in Fig. 3 in bcc metals are listed for comparison. The mean-absolute error (MAE) and root-mean-square error (RMSE) for the linear fittings are listed (in units of J/m^2). The deviation of $\delta_{fs}^{M/W}$ from $\delta_{gb(fit)}^{M/W}$ is shown in the parentheses.

M	Ref.	$\gamma_{fs(100)}$	$\gamma_{fs(110)}$	$\delta_{fs(100)}^{M/W}$	$\delta_{fs(110)}^{M/W}$	$\delta_{gb(fit)}^{M/W}$ (MAE, RMSE)	$\delta_{E_{coh}/a_0^2}^{M/W}$	$\delta_{a_0G_V}^{M/W}$	$\delta_{a_0c_{44}}^{M/W}$
W	PBEsol	4.40	3.63						
	PBEsol	4.36[a]	3.57[a]						
	PBE	4.02[b]	3.28[b]						
	EAM	3.90[c]	3.43[c]						
	Expt.	3.27[d]							
V	PBEsol	2.75	2.75	0.63 (28%)	0.76 (56%)	0.49 (0.10, 0.14)	0.74	0.28	0.18
	PBEsol	2.67[a]	2.66[a]	0.61[a]	0.75[a]		0.74[e]		
	EAM	2.78[c]	2.64[c]	0.71[c]	0.77[c]		0.65[f]	0.29[f]	0.26[f]
	Expt.	2.62[d]				0.67[g]	0.29[h]	0.27[h]	
Nb	PBEsol	2.57	2.27	0.58 (23%)	0.63 (32%)	0.47 (0.09, 0.11)	0.77	0.24	0.14
	PBEsol	2.60[a]	2.30[a]	0.60[a]	0.64[a]		0.75[d]		
	EAM	2.72[c]	2.49[c]	0.70[c]	0.73[c]		0.78[f]	0.26[f]	0.19[f]
	Expt.	2.66[d]				0.79[g]	0.27[h]	0.20[h]	
Ta	PBEsol	2.74	2.61	0.62 (9%)	0.72 (25%)	0.57 (0.10, 0.12)	0.91	0.48	0.56
	PBEsol	2.76[a]	2.60[a]	0.63[a]	0.73[a]		0.92[e]		
	EAM	3.04[c]	2.78[c]	0.78[c]	0.81[c]		0.84[f]	0.47[f]	0.55[f]
	Expt.	2.90[d]				0.86[g]	0.47[h]	0.56[h]	
Cr	PBEsol(NM)	4.13	3.70	0.94 (10%)	1.02 (20%)	0.85 (0.07, 0.09)	0.66	0.77	0.61
	PBEsol(NM)	4.03[a]	3.59[a]	0.92[a]	1.01[a]		0.64[e]		
	PBE(AFM)	3.06[b]	3.10[b]	0.76[b]	0.95[b]				
	EAM	2.30[c]	2.20[c]	0.59[c]	0.64[c]		0.56[f]	0.67[f]	0.58[f]
	Expt.	2.35[d]				0.57[g]	0.68[h]	0.58[h]	
Mo	PBEsol	3.54	3.10	0.81 (3%)	0.85 (9%)	0.78 (0.04, 0.05)	0.79	0.81	0.70
	PBEsol	3.60[a]	3.12[a]	0.83[a]	0.87[a]		0.79[e]		
	EAM	3.13[c]	2.89[c]	0.80[c]	0.84[c]	0.69[i]	0.78[f]	0.79[f]	0.70[f]
	Expt.	2.91[d]				0.79[g]	0.80[h]	0.76[h]	
Fe	PBEsol	3.12	2.92	0.71 (8%)	0.80 (22%)	0.66 (0.10, 0.12)	0.82	0.58	0.75
	PBEsol	3.04[a]	2.92[a]	0.70[a]	0.82[a]		0.80[e]		
	EAM	2.51[c]	2.36[c]	0.64[c]	0.69[c]	0.49[i]	0.59[f]	0.52[f]	0.68[f]
	Expt.	2.42[d]				0.60[g]	0.52[h]	0.68[h]	

[a]Ref. [57].
[b]Ref. [59].
[c]Ref. [60].
[d]Ref. [61].
[e]Ref. [62].
[f]Ref. [63].
[g]Ref. [64].
[h]Ref. [65].
[i]Ref. [43].

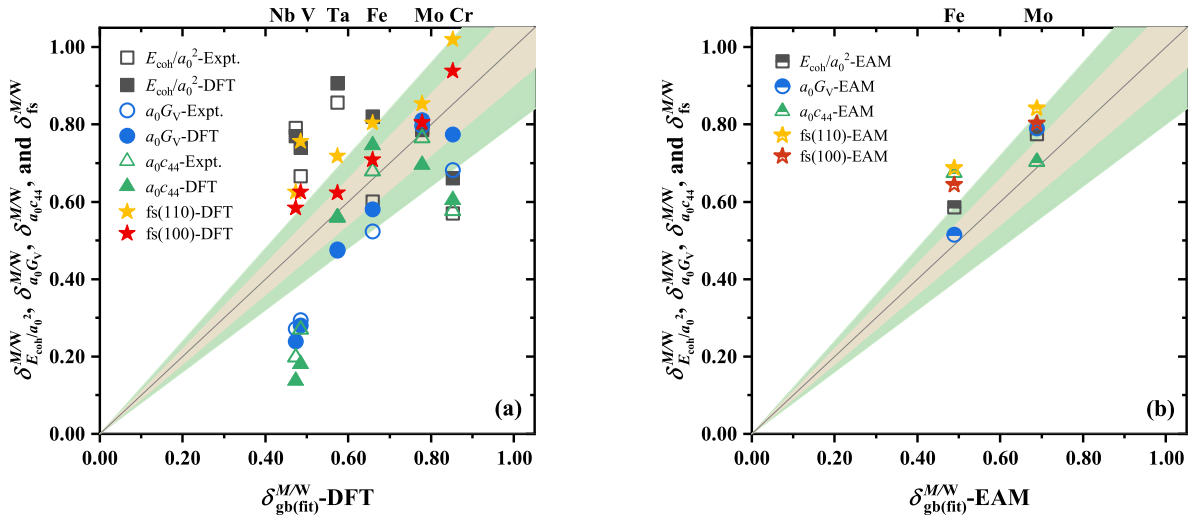

Fig. 4. Comparison of $\delta^{M/W}_{gb(fit)}$ with the ratios of the free surface energies, cohesive energy, shear modulus, and elastic constant. The present DFT results are plotted as solid symbols in (a). Shaded regions correspond to the deviations within 10% (light brown) and 20% (light olive), respectively. The relevant of ratios obtained from previous EAM are shown in (b) for comparison. All numerical values are listed in Table 2. (For interpretation of the references to color in this figure legend, the reader is referred to the web version of this article.)

Table 3
Calculated twin boundary energies (γ_{tw}, in units of J/m^2) for the studied bcc metals and their ratios relative to that of W ($\delta^{M/W}_{tw}$). Available DFT results from literature are listed for comparison.

M	γ_{tw}-Pres.	γ_{tw}-Ref.	$\delta^{M/W}_{tw}$
W	0.76	0.66 [56], 0.67* [44], 0.73* [66]	
V	0.37	0.26* [44]	0.48
Nb	0.25	0.25* [44]	0.33
Ta	0.30	0.29* [44]	0.39
Cr	0.74	0.65* [44]	0.97
Mo	0.58	0.54 [56], 0.48* [44]	0.76
Fe	0.46	0.51 [56], 0.42* [44], 0.47* [67]	0.61

DFT twin boundary energies calculated using the PBE approximation are marked with *.

4. Discussion

As briefly mentioned in the Introduction, it is not straightforward to compare the calculated (0 K, low Σ index GBs) and experimental (high temperatures, general GB) GBEs. It is essential to understand the critical difference between the obtained results. In the following, first we briefly review the two existing experimental methods for determining the general GBE (T.G. and Diff.). We will show that using these two methods, the calculated GBEs at elevated temperatures differ significantly from each other, and the obtained GBE calculated based on diffusivity data is almost two times of that from the thermal grooving experiments. This is distinct from the case for fcc metals where the two methods lead to consistent results [37]. The possible reasons for understanding the above discrepancy are discussed. Further, we will show that the general GBEs for the studied metals at 0 K can be estimated through the discovered scaling relationship using *ab initio* calculated surface energies. Finally, we predict the temperature-dependent GBEs using the Foiles's method [46] for pure metals and alloys. Comparison with the available experimental results in the literature shows satisfying agreement.

4.1. Experimental GBE measurement: the thermal grooving method

As briefly introduced in the Introduction, a few methods using experimental techniques are available to determine the GBEs (or the relative GBEs). The most 'direct' experimental method measures the geometry of GB grooves in thermal grooving experiments [6,68]. GBs exposed on the surface can form thermal grooves when annealing at elevated temperatures. According to Herring's equation which describes force relations at the GB-surfaces triple junction, at equilibrium conditions,

$$\sum_{i=1}^{3} \gamma_i \hat{\boldsymbol{t}}_i + \frac{\partial \gamma_i}{\partial \theta_i} \hat{\boldsymbol{n}}_i = 0, \tag{4}$$

where γ_i is the energy of the ith interface, $\hat{\boldsymbol{t}}_i$ and $\hat{\boldsymbol{n}}_i$ are forces tangential and normal to the interfaces, respectively, and $\partial\gamma_i/\partial\theta_i$ describes the torques applied to the interfaces. The torque, due to the anisotropy of the interfacial/surface tensions, tends to rotate the interfaces into positions of lower energy, approaching the equilibrium state. The torque terms can usually be neglected at equilibrium [8,69], then the above relationships are simplified as,

$$\gamma_{gb} = 2\gamma_{fs} \cos(\phi/2), \tag{5}$$

where ϕ is the dihedral angle at the groove, γ_{fs} is the free surface energy of the material. Notice that in Eq. (5) the groove is assumed symmetric and the FSEs of the two surfaces are identical, thus no crystal orientation dependence of FSE is considered. The crystallographic characteristics of the GBs in such measurements (e.g., for the purpose of measuring the general GBE of a polycrystal material) are usually not known in early zero-creep experiments using wires [20,68,70] and in multiphase equilibrium experiments using film samples [8–10]. We should emphasize here that not all types of GBs develop observable thermal grooves. In fcc metals, the coherent twins usually do not develop thermal grooves due to their low formation energies (i.e., usually less than ~100 mJ/m^2) [71].

In general, the above Herring's equations describe the relative relationships among the three interfacial energies at a triple junction. The three interfaces can be types of GBs, precipitate interfaces, surfaces, and solid/liquid interfaces [72]. At the GB/surfaces thermal grooves, they are the GBE and FSE. From the measured dihedral angles at those junctions, the relative ratios of GBE and FSE are calculated. When FSE and its temperature dependence are given/measured, the absolute GBE and its temperature variation can be obtained from the measured groove angles at various temperatures. The above procedure has been applied for various metals [8,13,17–19] and alloys [7,15].

Since only a limited number of GB grooves were measured, one should be careful in interpreting the obtained GBE by Eq. (5). Usually, from the histogram of the measured groove dihedral angles and the occurrence frequency, the median/mean value of the angle ϕ is

obtained. Then the calculated GBE is considered as the representative value for a general GB. Therefore, the larger number of the examined GB grooves, the better the reliability of the obtained GBE. Recently, Haremski et al. [37] measured the thermal groove angles in a large population in Ni by atomic force microscopy. Particularly, the distributions of the dihedral angles (therefore the relative GBEs) were studied in categories of high-angle GBs (HAGB), low-angle GBs (LAGB), and $\Sigma 3$ GBs (including both coherent and noncoherent twin boundaries). It is important to notice that the proportion of the distinct GBs in length was measured to be ~45% for $\Sigma 3$ GBs, ~45% for HAGBs, and ~10% for LAGBs. Within the $\Sigma 3$ GBs, about half was coherent twin boundary. From the dihedral angle distribution for the HAGBs, the mean value of the angle was calculated and the corresponding GBE was found to be in good agreement with previous results from thermal grooving experiments [8,20]. Notice that those early experiments [8,18–20] measured the randomly picked GB grooves (usually for a number ~50 or fewer) and calculated the median (or mean) of the dihedral angles from their occurrence frequency, and in some studies it was explicitly stated that only well-developed grooves (i.e., large GBE) were chosen [10]. Both LAGBs and $\Sigma 3$ GBs showed a strong inverse relationship between the occurrence frequency and the GBE, i.e., the coherent twin is the most popular one, which has the lowest energy. This observation is generally applied in fcc metals and alloys from a series of experimental studies [73,74]. The mean GBE of LAGBs was found about half of that for HAGBs in Ni [37]. The coherent twin boundary energies for fcc metals and alloys are usually one order of magnitude smaller than that for random oriented GBs. In thermal grooving experiments, the coherent twin boundaries develop no vicious grooves if not, i.e., ϕ close to 180°. From the above studies, one sees that the reported GBEs in fcc materials based on the thermal grooving method, particularly the early studies which examined a very limited number of thermal grooves [8,20], should be interpreted as the typical/representative value for the most frequently observed randomly orientated GBs (with large energies). This observation is also supported by the fact that the GBEs for fcc materials from thermal grooving experiments closely agree with the results calculated by Borisov's model, which will be discussed in the later sections. We emphasize here that the low-energy GBs like the coherent twin can be easily excluded in thermal grooving experiments for the determination of the general GBE in fcc materials, despite their high fraction (/occurrence frequency).

The situation is distinct in bcc materials. Using the 3D EBSD technique, the five degrees of freedom of the GBs can be identified and the GB character distribution was extensively studied in both fcc [75,76] and bcc [43] metals. Rohrer et al. [3] showed that a general inverse relationship exists between the frequency (or the population) and the GBE. In bcc metals, the $\Sigma 3(112)$ twin is usually found having the lowest energy by both experiments [77,78] and theoretical studies [79,80]. However, this twin boundary energy in bcc metals is about 1/5–1/4 of those of HAGBs, which remarkably differs from the case of fcc metals, i.e., the fcc twin boundary energy is one order of magnitude smaller than the general GBE [10,81]. Furthermore, there are several low Σ GBs with high number of coincidence sites having competing low energies as $\Sigma 3(112)$ [43]. Because of the high energy of the twin boundary in bcc metals, Nilles and Olson [77] showed that the thermal grooving method can also be applied to determine the twin boundary energy. Therefore, the grooves with the largest observed dihedral angles are likely corresponding to (/close to) the $\Sigma 3(112)$ twin boundary (or GBs with similar energies) in bcc metals. We re-examined the thermal grooving results for bcc metals available in literature [18], and calculated the GBEs corresponding to the largest observed angles. For W, Mo, Nb, and Ta, the energies are 0.79, 0.36, 0.44, and 0.56 J/m^2, respectively, at 1500 °C, which compare well with the calculated $\Sigma 3(112)$ twin boundary energies (0.76 J/m^2 for W, 0.58 J/m^2 for Mo, 0.25 J/m^2 for Nb, and 0.30 J/m^2 for Ta, obtained by DFT at 0 K (Table 3) and 0.66 J/m^2 for W, 0.47 J/m^2 for Mo, 0.30 J/m^2 for Nb, and 0.24 J/m^2 for Ta at 1500 °C after considering the temperature dependence (i.e., assuming the same temperature dependence for twin and general GBEs, see discussions in Section 4.5)). However, in bcc metals, the fraction of twin boundary is not significantly high, usually less than 1%–2% [82,83], comparing to the twin fraction of 20%–50% in fcc materials (depending on i.e., the stacking fault energy). The grain boundary plane distribution in a commercial interstitial-free steel revealed a relatively low anisotropy with a tendency for grain to terminate on low index planes, and the most common grain boundary plane was (111), despite the $\Sigma 3(112)$ boundary has the lowest energy [82,83]. Considering the general inverse correlation between the GBE and the measured population [3], the thermal grooves examined in bcc metals must include general high-angle GBs and the low-energy GBs like the $\Sigma 3(112)$ twin. This is significantly different from the fcc case where the low-energy twin boundary with the largest population is always excluded from the groove angle statistics. From a statistical point of view, in bcc metals, the thermal grooves for GBs with lower energies should be more frequently met than those with higher energies, thus, the groove angle distribution will be skewed to the high angle direction, consequently, the median (/mean) angle from the groove angle-frequency statistics will be systematically higher than those in fcc metals.

4.2. Experimental GBE determination: the Borisov's method

Considering that both the activation energy of diffusion and GBE are intrinsically related to the atomic binding forces within the GB region, it was expected that a relation between the increased atomic mobility in the self-diffusion at the GB and the GBE might exist. Borisov et al. [31] first treated this problem and showed that the GBE may be regarded as half the difference in the free energy of activation for atoms diffusing in the GB and in the lattice. Assuming the arbitrary high-angle GBs with a width equal to one atomic diameter and with an average population of one atom per unit cell (i.e., approximately by the lattice parameter squared, a^2), the GBE may be expressed as

$$\gamma_{gb} = \frac{RT}{2a^2 N_A}(\Delta G_v - \Delta G_{gb}), \tag{6}$$

with $\Delta G_{gb} = \Delta H_{gb} - T\Delta S_{gb}$ and $\Delta G_v = \Delta H_v - T\Delta S_v$, where ΔH and ΔS are the corresponding enthalpy and entropy terms (in units of J/m^2) for GB and lattice diffusion, respectively. The diffusion coefficients of GB and lattice are usually taking the Arrhenius form,

$$D = D^0 \exp(-\Delta H/RT), \tag{7}$$

where D^0 is the temperature independent term. According the atomic theory of diffusion, $D^0 = g\lambda^2 f\nu \exp \Delta S/RT$, where g is the geometrical factor, λ is the jump distance, f is the correlation factor for tracer diffusion, ν is the jump frequency. When it is assumed that the non-exponential terms above are identical for both GB and lattice diffusion, then neglecting the differences in the vibrational entropies for GB and volume diffusion and substituting Eq. (7) in the corresponding places in Eq. (6), one can arrive at,

$$\gamma_{gb} = \frac{RT}{2a^2 N_A} \ln \frac{D_{gb}}{D_v} = \frac{1}{2a^2 N_A}[RT \ln \frac{D^0_{gb}}{D^0_v} + (\Delta H_v - \Delta H_{gb})]. \tag{8}$$

In the above expressions, N_A is Avogadro's number, D_{gb} and D_v are diffusivity coefficients for GB and bulk diffusion, respectively. From the above equations, one notices that the linear temperature-dependence of GBE is assumed and given by $R/(2a^2N_A)\ln(D^0_{gb}/D^0_v)$ and the 0 K GBE is given by $(\Delta H_v - \Delta H_{gb})/(2a^2N_A)$. More details about the physical understanding of the above model can be found in Refs. [31,33].

Notwithstanding the assumptions made above, Eq. (8) was demonstrated very successfully the calculation of the GBEs for fcc metals [35,37,38], reaching a close agreement with those obtained from thermal grooving experiments. However, large discrepancies between the two sets of 'experimental' results are noted in the bcc and hexagonal close-packed (hcp) metals [35]. Pelleg showed that in δ-Fe the Borisov's

model overestimates the GBE quite significantly, which was ascribed to a reason that the fortuitous cancellation of the non-exponential terms in Eq. (7) in driving Eq. (8) is not satisfied in the bcc/hcp structures [33]. Obviously, it is problematic to define a reliable atomic density at the GBs in hcp structure from a single lattice parameter as assumed for fcc and bcc lattices (Eq. (6)) [35]. We emphasize here that Eq. (6) assumes the same atomic density for the GB structure, i.e., one atom per a^2, in both fcc and bcc materials, which is however not properly justified.

Another important aspect when applying the Borisov's model and interpreting the obtained GBE values is related to the experimentally measured self-diffusivity at GB D_{gb}. The GB diffusivity is usually determined by the radiotracer technique [39,84] using samples with a large fraction of high-angle GBs. D_{gb} is calculated from the penetration profile at a specific temperature using the sectioning method. For example, when diffusion kinetics follows the C-type regime (where primarily GB diffusion dominates), which is usually fulfilled at low temperatures and short times of diffusion annealing, $D_{gb} = (-\partial \ln \bar{c}/\partial y^2)^{-1}/(4t)$, where t is diffusion time, $\bar{c}$ and y are the tracer concentration in a section and the penetration depth, respectively. In the course of deriving the above relation between diffusivity and measured parameters, GB is treated as a uniform and isotropic slab of material of width 0.5 nm within which diffusion occurs with a large coefficient [85]. It is consistent with experiments that the GB width was measured to be about 0.5 nm in a number of fcc metals and alloys [39,40]. The special GBs like $\Sigma 3$ and $\Sigma 11$ [110] tilt GBs which are closed or relatively closed-packed GBs lead to slower diffusivities compared to other high-angle GBs with more open structures. Explicitly, Herbeuval [86] measured the relative diffusivity of [110] symmetric tilt GBs in Al and found minimum diffusivities at $\Sigma 3$ and $\Sigma 11$ boundaries. Therefore, despite that these types of special GBs may occur more often due to their lower GBEs [38], they do not contribute to the large difference in diffusivity between GBs and bulk [87]; and their effect on the shallow part of the penetration profile is not included when fitting the tails of the penetration profile for the determination of diffusivity [38].

A remark is due here. It is often assumed that a kind of an 'averaged' GB diffusivity, i.e. an averaged value of the triple products, $P = s\delta D_{gb}$, at elevated temperatures (the B-type kinetic regime) or that of the GB diffusion coefficients, D_{gb}, at low temperatures (the C-type regime), is measured in a typical tracer experiment in a polycrystalline material when the whole spectrum of GBs is present, from low-angle to high-angle GBs including possible special grain boundaries. It is generally not true and the situation depends strongly on the ratio of the GB diffusion depth, Λ, and the grain size, d. In a typical GB diffusion experiment for a coarse-grained polycrystalline material, $\Lambda < d$ (often $\Lambda \ll d$) and a tracer diffusion experiment corresponds effectively to diffusion in a set of parallel (and almost perpendicular to the outer surface due to a homogenizing heat treatment) GBs. Using the parallel sectioning of the whole sample, one averages effectively the *concentration distributions* around all different GBs (but not their diffusivities) and determines the slope of the deepest part. That slope corresponds to the contribution of the fastest GBs present in the polycrystalline material and characterizes 'general high-angle GBs' [88]. A good reproducibility of the results for GB diffusion in a polycrystalline material reported by different researchers, e.g. for Ag GB self-diffusion in polycrystalline Ag of nominally the same 5N purity, as it was discussed in Ref. [89], confirms this viewpoint.

Consequently, the measured GB diffusivity corresponds to the highest value for the general high-angle GBs with open structures. When adopting such GB diffusivity data to determine the GBE according to the above Borisov's equation, the obtained GBE should be interpreted as the high-end value for the GBs with probably the most open structures [33, 39].

4.3. Experimental GBEs: the case of W

The two sets of the experimental GBEs for W are presented in Fig. 5b. All numerical values are listed in Table S3 in SM. The experimental GBEs from the two methods discussed above differ clearly from each other, i.e., by approximately a factor of two, but exhibit a similar decreasing trend with increasing temperature. Similar deviation is also found for other bcc metals, see e.g. Mo and Fe in Fig. 6, for which both two sets of experimental results are available.

Foiles studied the temperature dependence of GBE in Ni and showed that the GBE and the elastic constant c_{44} share approximately the same temperature dependence up to about 0.75 of the melting temperature. Specifically, the relationship is expressed as,

$$\gamma_{gb}(T) = \gamma_{gb}(T_0)\frac{a(T)c_{44}(T)}{a(T_0)c_{44}(T_0)}, \tag{9}$$

where a is the lattice constant and ac_{44} has the same unit as the GBE (energy per area), T_0 is a reference temperature and was originally set at room temperature. Scheiber et al. [45] recently assessed the approach in W and showed that the above model leads to a quantitative agreement with the temperature dependence of the GBEs obtained by *ab initio* calculations using the quasiharmonic approximation. Here, using experimental c_{44} from Refs. [90–92] and $a(T)$ calculated from the linear thermal lattice expansion method, i.e., $a(T) = a_{300}(1 + \alpha \Delta T)$ with $\alpha = 4.6 \times 10^{-6}$/K and the room temperature lattice parameter ($a_{300} = 3.16$ Å) [64], we derive the temperature dependence of ac_{44} (Fig. 5a) and apply the Foiles's approach to obtain the temperature dependence of the GBE (Fig. 5b). The two sets of experimental results are fitted to Eq. (9) separately, and two GBEs at 0 K are obtained, 2.30 J/m^2 and 1.21 J/m^2, respectively for the Borisov's method (Diff.) and for the thermal grooving method (T.G.). The quality of the fittings is very good with RMSE of 0.005 J/m^2 for T.G. and 0.008 J/m^2 for Diff., respectively.

Alternatively, one might simply fit the high-temperature experimental results by a linear function. In particular, in the Borisov's method, the temperature dependence of the GBE is in fact assumed linear. For W, linear extrapolation of the high-temperature results from the two sets of the experiments to 0 K results in 2.43 J/m^2 for Diff. and 1.08 J/m^2 for T.G., respectively. However, one will find that very often it is impossible to derive the low-temperature GBE in this way when high-temperature results are rare. In the following, we will assess an alternative method for predicting the general GBE at 0 K based on the scaling relationship of the GBEs in materials with the same crystal structure, as revealed in Section 3.2 [41,43,58,81].

4.4. General GBE of bcc metals at 0 K

As demonstrated in Section 3.2, the GBEs of the boundaries with the same structures in a pair of bcc metals are correlated by a material dependent constant via $\gamma_{gb}^{A} = \delta\gamma_{gb}^{B}$. Similar observation was made between Fe and Mo with a large number of GBEs calculated by EAM method [43]. In our recent DFT studies for fcc metals, similar results were obtained [58]. The findings suggest that if the scaling factor δ is obtained, for example, from fitting the calculated GBEs of a selected group of GBs in a pair of metals as shown in Fig. 3, then δ may be used for the prediction of other GBEs which have been studied in a reference metal. As discussed in Section 3.2, we find that δ is approximately given by the ratio of the low-index FSE in a more reliable way than other previously proposed parameters like the ratios of cohesive energy or shear moduli.

More interestingly, the scaling relationship may be used for the prediction of the general GBE. As discussed previously, one may assume that an experimental method for determining the GBEs of polycrystal materials with the same crystal structure measures the general GBs with the same effective structure. Therefore, the experimental general GBEs will be scaled by the same δ as for the tilt and twist GBs, i.e.,

$$\gamma_{gb}^{expt.A} = \delta\gamma_{gb}^{expt.B}. \tag{10}$$

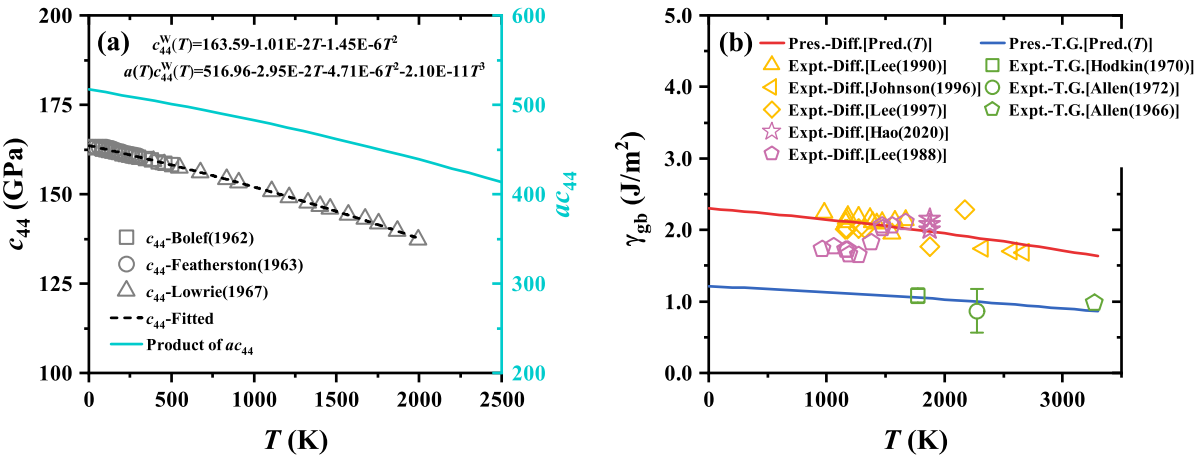

Fig. 5. (a) Temperature dependence of c_{44} [90–92] from experiments, and the product of ac_{44} for bcc W. The temperature dependence of the lattice parameter is calculated using the linear thermal lattice expansion. (b) The temperature dependence of the general GBE for W based on results from the Borisov's method [93–95] and from the thermal grooving experiments [18,19,70]. In (b), the $\gamma_{gb}^{Expt.-Diff.}$ results (purple symbols) calculated using the diffusivities of alloying elements (Mo [96] and Co [97] tracers in W) other than the self-diffusivity are also included for comparison. Notice that these data points are not included for fitting to obtain the 0K GBE value. (For interpretation of the references to color in this figure legend, the reader is referred to the web version of this article.)

Table 4
The predicted general GBEs at 0 K according to the scaling relationship. Here, $\gamma_{gb}^{Pred.}(\delta_{fs(100)}^{M/W})$ and $\gamma_{gb}^{Pred.}(\delta_{gb(fit)}^{M/W})$ are the predicted GBEs using the (100) FSE ratio and the gradient of the linear fitted GBEs as the scaling prefactor δ, respectively. The experimental general GBEs at 0 K for W from Borisov's (Diff.) and thermal grooving (T.G.) methods are used as the reference values, respectively. $\overline{\gamma_{gb}^{Calc.}}$ is the equal-weight average over the calculated large-angle GBEs excluding the $\Sigma3(112)$ twin boundary energy. The relative errors relative to $\gamma_{gb}^{Pred.-Diff.}(\delta_{fs(100)}^{M/W})$ are listed in parentheses.

M	$\gamma_{gb}^{Pred.-T.G.}(\delta_{fs(100)}^{M/W})$ (0 K) (J/m^2)	$\gamma_{gb}^{Pred.-T.G.}(\delta_{gb(fit)}^{M/W})$ (0 K) (J/m^2)	$\gamma_{gb}^{Pred.-Diff.}(\delta_{fs(100)}^{M/W})$ (0 K) (J/m^2)	$\gamma_{gb}^{Pred.-Diff.}(\delta_{gb(fit)}^{M/W})$ (0 K) (J/m^2)	$\overline{\gamma_{gb}^{Calc.}}$ (0 K) (J/m^2)
W	1.21		2.30		2.61 (14%)
V	0.76	0.59	1.44	1.12	1.33 (−8%)
Nb	0.71	0.57	1.34	1.09	1.23 (−9%)
Ta	0.76	0.70	1.43	1.32	1.50 (5%)
Cr	1.14	1.03	2.16	1.96	2.27 (5%)
Mo	0.98	0.94	1.85	1.79	2.04 (10%)
Fe	0.86	0.80	1.63	1.52	1.68 (3%)

In our previous work, we showed that in fcc metals the above assumption is not unreasonable and the predicted GBs are in a close agreement with experiments [58]. The above assumption is also justified by the observed GB character distribution [3]. Beladi et al. [83] showed that the polycrystals with the same atomic structure have very similar GB character distribution (GBCD) and GBE distribution characteristics. Liu et al. found that GBCD in W is close to that in a ferritic steel [98].

Taking W as the reference, the general GBEs at 0 K for bcc metals are calculated accordingly and listed in Table 4. Here, the ratio of the (100) FSE ($\delta_{fs(100)}^{M/W}$ in Table 2) is used as the scaling factor δ. Depending on which experimental GBE of W is referred to, T.G. or Diff., two sets of general GBEs at 0 K are reported here. In principle, one may compare the predicted results with the 0 K experimental values extrapolated from high temperature results (as done for fcc metals in Ref. [58]), however, such data points are very few for bcc metals, which makes such extrapolation unreliable. As discussed in Section 4.2, the general GBE estimated by the Borisov's method corresponds to the GBs with the largest energies, which implies that if we average the DFT calculated GBEs for the large-angle GBs (θ), the obtained results should be comparable with $\gamma_{gb}^{Pred.-Diff.}$ (0 K). In Table 4, the mathematically averaged GBEs ($\overline{\gamma_{gb}^{Calc.}}$) from the studied [110] tilt GBs in Fig. 2, excluding the $\Sigma3(112)$ twin boundary, generally agree with the $\gamma_{gb}^{Pred.-Diff.}$ (0 K) values with an error less than ~10%. We may emphasize here that $\overline{\gamma_{gb}^{Calc.}}$ in Table 4 should only be considered as a rough estimation of the general GBE towards the upper limit considering the limited number of GBs included in averaging.

4.5. Predicting the temperature dependent general GBE for bcc metals

In the following section, we start with these predicted 0 K values and follow the Foiles's method to predict the GBEs at elevated temperatures, then we compare our predictions with available experimental results at high temperatures. The calculated temperature dependence of general GBEs for six bcc metals are presented in Fig. 6. Available experimental data are shown as open symbols and their numerical values are listed in Table S3 in SM. The predicted γ_{gb} at 0 K based on the scaling relationship with $\delta_{fs(100)}^{M/W}$ in Table 4 are marked as the stars in the plots. In general, good agreement is reached between the predicted and experimental GBEs obtained at elevated temperatures. Detailed discussions are given in the following.

For V, Nb, and Ta, we observe an anomalous behavior of the temperature dependence, which is distinct from the nearly linear temperature dependence of the GBE in fcc metals at high temperatures. This is primarily because of the peculiar temperature dependence of the shear constant c_{44}. The general trend of the temperature-dependent c_{44} for cubic metals typically shows a monotonically decreasing trend with increasing temperature. However, previous experimental measurements found that c_{44} values for transition metals of V [112], Nb [113], and Ta [114] have a peculiar temperature behavior, which decreases as T^4 at low temperatures. Experiments reported that this anomaly in temperature variation is mainly attributed to the Fermi surface, which was demonstrated later by theoretical evaluations of the band structure [115]. Recent theoretical studies [116,117] have made efforts to understand the anomalous thermoelastic behavior for these transition metals at the atomic scale using DFT calculations and have shown that

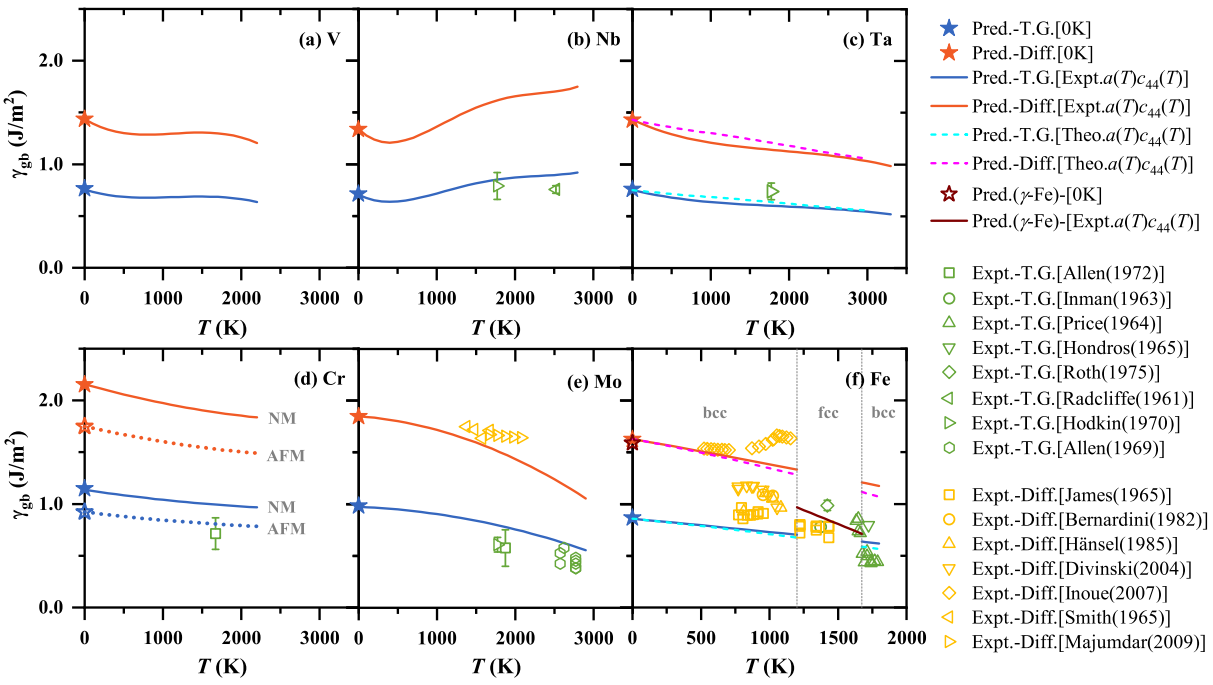

Fig. 6. Temperature dependence of general GBEs in bcc metals. The open symbols represent the measured general GBEs in Cr [19], Nb [18,99], Mo [17–19], Ta [18], and Fe [13,16,20,100–105] using the thermal grooving (green) and Borisov's (yellow) methods. Experimental data of diffusivity and GBEs are also available in Table S3 in SM. The solid stars represent the predicted γ_{gb} at 0 K based on the scaling relationship using the ratios of the (100) surface energies as the scaling prefactor. For Cr, the 0 K general GBEs are different for using the antiferromagnetic (AFM) and non-magnetic (NM) surface energies, respectively, emphasizing the magnetic effect on the GBEs. Here, the reference surface energies are taken from Ref. [59] and calculated with the PBE approximation. In (f), the GBE for fcc Fe at 0 K is predicted from the surface energies for Cu [59] and γ-Fe [106], and the reference experimental GBE of Cu [58]. The temperature dependence (purple line) is estimated from the experimental temperature-dependent $a(T)c_{44}(T)$, where $a(T)$ and $c_{44}(T)$ are from Refs. [107–109]. In (c) and (f) we also show the temperature dependence of the GBEs (dashed line) based on the theoretical $a(T)c_{44}(T)$ from Refs. [110,111]. (For interpretation of the references to color in this figure legend, the reader is referred to the web version of this article.)

the anomalous behaviors of c_{44} depend on the electronic entropy contribution. Therefore, one should be careful when fitting the temperature dependence of c_{44} in these metals. The temperature dependence of the GBE might be also affected by the anomalous electronic structures at high temperatures. We therefore employ the polynomial fitting of T^4 for the collected experimental data. The detailed fitting results are presented in Fig. S4a in SM. Based on the above fittings, we find that the predicted temperature dependence of GBEs for Nb and Ta agrees well with available experimental measurements [18,99] in Fig. 6b and c.

For Fe, Cr, and Mo, the temperature variations of c_{44} were fitted to the second order of temperature T^2. More details can be found in Fig. S4b in SM. Compared to the two sets of experimental results for Mo (Fig. 6e), the presently obtained theoretical predictions agree well with both T.G. [17–19] and Diff. [118,119] values. For Cr and Fe, attention should be paid to magnetism. We recall that the present calculations for Cr GBEs and FSEs are nonmagnetic, whereas the antiferromagnetic state is physically more relevant for Cr, which is probably responsible for the large deviation between the present prediction and the experimental GBE at high temperatures [19]. In Table 2, the nonmagnetic calculations yielded a larger (100) FSE (4.13 J/m^2) for Cr compared to 3.06 J/m^2 [59,120] obtained for the AFM state and 2.53 J/m^2 [61] from experimental measurements. This is because of the reduced coordination at the free surface and hence the increased magnetic moments at the surface, leading to a lower FSE [120]. Similar magnetic effect is expected for general GBs with reduced coordinations. However, one notices that at the same NM state, the $\delta^{M/W}_{gb(fit)}$ and $\delta^{M/W}_{fs(100)}$ or $\delta^{M/W}_{fs(110)}$ values are close to each other (see values in Table 2) which indicates that the scaling relationship is still valid for NM Cr as for other bcc metals. As a consequence, neglecting magnetism of Cr overestimates the scaling prefactor $\delta^{M/W}_{fs(100)}$, and the corresponding predicted general GBE at 0 K. Indeed, when we adopt the AFM surface energy of Cr [59] to calculate δ, the predicted GBE (dashed lines in Fig. 6d) agrees better with the available experimental point at a high temperature.

The experimental GBEs for Fe (Fig. 6f) show the largest scatter in the studied bcc metals, especially for those calculated by diffusivity data. It is due to the fact that there is a large scatter of 3–4 orders of magnitude in the self-diffusivity of bcc Fe at identical temperatures [102–105,121–124]. Those differences were associated with various factors, such as the purity of specimens and the microstructure of GB region. Specifically, the purity of samples was shown to have significant effects on the measured GB diffusivity in Ni [38,39]. Surholt [125] also demonstrated that the residual impurity of sulfur in high-purity polycrystalline Cu can significantly affect the activation enthalpy of GB self-diffusion. Further, Divinski [104] argued that dislocations attached to GBs can strongly influence the measured GB diffusivity. With above points mentioned, it is not surprising to see that the diffusivity-based GBE calculation in bcc Fe leads to very large scatter in Fe. Particularly, the $\gamma^{Diff.}_{gb}$ values calculated based on the GB diffusivity data from James et al. [101] are noticeably smaller than others, but close to the GBE values from the thermal grooving experiments. However, considering the observation that in other bcc metals $\gamma^{Diff.}_{gb}$ is usually larger than $\gamma^{T.G.}_{gb}$ by a factor ~2, the James' diffusivity results are considered unreliable. The $\gamma^{Diff.}_{gb}$ results calculated with diffusivity data from Dinviski et al. [104], Bernardini et al. [102] and Hänsel et al. [103] agree with each other. Results from Inoue et al. [105] data agree better with our predictions at low temperatures, but deviate at temperatures around T_C due to the diffusivity anomaly of magnetism-origin. However, there are still debates on the transitions in the GB and bulk diffusivities at around T_C [104,126]. The GBEs from thermal grooving experiments are only available above T_C, but they all show a good agreement with our predicted results in both fcc and bcc Fe. Particularly, the two experimental methods lead to consistent results for fcc Fe.

Before we close this section, we may point out that instead of using the experimental $a(T)c_{44}(T)$ data for estimating the temperature

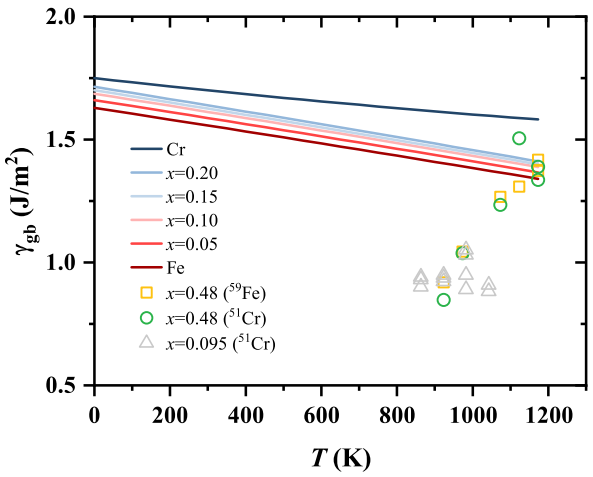

Fig. 7. Predicted GBEs for $Fe_{1-x}Cr_x$ ($0 \leqslant x \leqslant 0.2$) as a function of temperature. The temperature-dependent GBEs for pure Fe and Cr are taken from the Diff. predictions in Fig. 6(d) and (f). Here, the variation of the surface energies of $Fe_{1-x}Cr_x$ alloys with respect to Cr concentrations is from Ref. [131]. The temperature dependence of the GBE of $Fe_{1-x}Cr_x$ alloys is assumed the same as that for α-Fe. Available experimental general GBEs for Fe-Cr alloys calculated by the Borisov's method using the measured diffusion coefficients by Fe and Cr tracers [132,133] are shown for comparison.

dependence, one may also use the $a(T)c_{44}(T)$ results from *ab initio* [45, 127,128] or empirical potential [46,129] calculations, so the proposed approach for the general GBE prediction can rely less on experimental input except for the experimental data for the reference metal. However, DFT calculations for considering the temperature effects on elastic constants are usually complicated (see, for example, Refs. [45, 130]), here we adopt the available DFT results of elastic constants in Refs. [110,111] and demonstrate for the cases of Ta and Fe. The polynomial fittings to the elastic constants are plotted in Fig. S5 in SM. In Fig. 6c and f for Ta and Fe, we present the predicted temperature-dependent GBEs using the theoretical $a(T)c_{44}(T)$ (dashed lines), which are in satisfying agreement with the results using the experimental elastic constants.

4.6. Predicting general GBEs of Fe-Cr alloys

In a previous study, we demonstrated that the scaling relationship between the GBEs in different metals is of particular importance for the prediction of GBEs of alloys [58], considering the fact that both thermal grooving experiments and diffusivity measurements involve treatments at high temperatures which can result in significant GB diffusion and segregation. Despite that the predicted general GBEs at 0 K for Fe–Cr–Ni stainless steels were found in good agreement with the extrapolated experimental data, one should interpret the results with caution because no alloying segregation at GB or surface was considered when using the scaling method to predict the general GBE. With that said, applying the current method for predicting the general GBE for ideal solid solutions provides representative values for homogeneous alloys, which is important for further studies. Considering that all segregation processes tend to decrease the excess energy, here our predicted GBE should be considered as the upper limit for the general GBE, which can be improved when alloy segregation energies and profile are known.

In the following, we first predict the general GBEs at 0 K for Fe-Cr ferritic steels according to the scaling relationship using the calculated (100) surface energies and the experimental $\gamma_{gb}^{Diff.}$ of W at 0 K as the reference. The temperature dependence of GBE is assumed the same as α-Fe shown in Fig. 6f. The reason for the simplification is due to the lack of experimental $c_{44}(T)$ data for Fe-Cr alloys. The results for $Fe_{1-x}Cr_x$ alloys are presented in Fig. 7 for Cr concentrations of 0.05, 0.10, 0.15, and 0.20. With increasing Cr, the general GBE gradually increases between the Fe and Cr GBEs. This is contrary to the results by molecular dynamics (MD) calculations in Ref. [134], where they reported a decreasing trend of GBE with increasing Cr composition. One should notice that *ab initio* calculations predict higher surface energies and GBEs of Cr than the counterparts of Fe for the same defect structures (see Figs. 2 and 3 and Ref. [120]), while the MD calculations predicted the opposite trend [134]. The failure of the empirical potential studies of GBEs highlights the importance of the proposed method for predicting GBEs with accurate *ab initio* methods.

As the presented example above, once the concentration dependence of FSE and temperature dependence of ac_{44} are determined, we can provide a parameterized function for predicting the GBE with respect to both the chemical and temperature variations. Using the calculated FSEs by Schönecker et al. [131], the following regression function for the (100) FSE with respect to the composition in $Fe_{1-x}Cr_x$ alloys is obtained,

$$\gamma_{fs(100)} = 3.117 + 1.348x - 2.667x^2 \ (\mathrm{J/m^2}), \tag{11}$$

with x up to 0.2 (i.e., 20 at.% Cr). Then, adopting the same temperature dependence for bcc Fe (see also discussion and calculation detail in SM), the temperature-dependent general GBE of $Fe_{1-x}Cr_x$ alloys is predicted,

$$\gamma_{gb}(x,T) = (1.629 + 0.704x - 1.394x^2) \times (1 - 1.446 \times 10^{-4}T - 5.396 \times 10^{-9}T^2) \ (\mathrm{J/m^2}). \tag{12}$$

The prediction is considered valid for $0 \leqslant x \leqslant 0.20$ and $0 \leqslant T \leqslant T_C$.

5. Summary

Using *ab initio* calculations, we determine the GBEs of seven bcc transition metals for 10 types of symmetric tilt GB structures. The calculated GBEs show an excellent agreement with previous theoretical results and establish a solid base for exploring the correlation among the GBEs of different metals. Other physical properties, e.g., elastic constants, cohesive energies, and surface energies for the selected metals are also computed. Compared to the ratios of the GBEs of a pair of metals, we find that the ratios of FSE of bcc metals have a better agreement with the scaling prefactor δ than other parameters based on shear modulus, elastic constant, and cohesive energy as proposed in the previous studies. With the above findings, we propose a method for predicting the general GBE at 0 K, which also enables the prediction of general GBEs at finite temperatures when adopting the Foiles's method for treating the temperature dependence of GBE. We demonstrate the proposed approach for the studied bcc metals and observe generally good agreement with available experimental GBEs at elevated temperatures. Furthermore, we carefully review the two common experimental methods for assessing the general GBEs and find a huge difference in the results from the approaches for bcc metals. The fundamental reasons are carefully discussed. Finally, we discuss the application of the proposed method for predicting the general GBEs in the ferritic Fe-Cr alloys when no GB segregation is considered. The present systematic study establishes an accurate and reliable *ab initio* model for predicting the temperature-dependent GBE in bcc metals with the possibility to extend its application in alloys when GB segregation is further studied.

Declaration of competing interest

The authors declare that they have no known competing financial interests or personal relationships that could have appeared to influence the work reported in this paper.

Acknowledgments

The present work is performed under the project "SuperFraMat" financed by the Swedish Steel Producers' Association (Jernkontoret) and the Swedish Innovation Agency (Vinnova). C.L., S.L., and L.V. acknowledge the Swedish Research Council, the Swedish Foundation for Strategic Research, the Swedish Foundation for International Cooperation in Research and Higher Education, the Hungarian Scientific Research Fund (OTKA 128229), and the Carl Tryggers Foundation for financial support. C.L. also acknowledges the financial support from the China Scholarship Council, the Swedish Steel Producers' Association (Jernkontoret), the Axel Hultgrens Fond, and the Axel Ax:son Johnsons Forskningsfond. S.D. acknowledges the financial support from the German Science Foundation (DFG) via a research grant DI 1419/19-1. The computations were enabled by resources provided by the National Academic Infrastructure for Supercomputing in Sweden (NAISS) at the National Supercomputer Centre (NSC) in Linköping partially funded by the Swedish Research Council through grant agreement no. 2022-06725.

Appendix A. Supplementary data

Supplementary material related to this article can be found online at https://doi.org/10.1016/j.actamat.2023.119074.

References

[1] V. Randle, G. Owen, Mechanisms of grain boundary engineering, Acta Mater. 54 (7) (2006) 1777–1783, http://dx.doi.org/10.1016/j.actamat.2005.11.046.
[2] T. Watanabe, Grain boundary engineering: historical perspective and future prospects, J. Mater. Sci. 46 (12) (2011) 4095–4115, http://dx.doi.org/10.1007/s10853-011-5393-z.
[3] G.S. Rohrer, Grain boundary energy anisotropy: A review, J. Mater. Sci. 46 (18) (2011) 5881–5895, http://dx.doi.org/10.1007/s10853-011-5677-3.
[4] D. Raabe, M. Herbig, S. Sandlöbes, Y. Li, D. Tytko, M. Kuzmina, D. Ponge, P.P. Choi, Grain boundary segregation engineering in metallic alloys: A pathway to the design of interfaces, Curr. Opin. Solid State Mater. Sci. 18 (4) (2014) 253–261, http://dx.doi.org/10.1016/j.cossms.2014.06.002.
[5] J. Han, S.L. Thomas, D.J. Srolovitz, Grain-boundary kinetics: A unified approach, Prog. Mater. Sci. 98 (2018) 386–476, http://dx.doi.org/10.1016/j.pmatsci.2018.05.004.
[6] C. Herring, The Physics of Powder Metallurgy, McGraw Hill, New York, 1951.
[7] J. Kudrman, J. Čadek, Relative grain boundary free energy and surface free energy of some metals and alloys, Czech. J. Phys. B 19 (11) (1969) 1337–1342, http://dx.doi.org/10.1007/BF01690833.
[8] L.E. Murr, R.J. Horylev, W.N. Lin, Interfacial energy and structure in FCC metals and alloys, Phil. Mag. 22 (177) (1970) 515–542, http://dx.doi.org/10.1080/14786437008225841.
[9] L.E. Murr, Twin boundary energetics in pure aluminium, Acta Metall. 21 (6) (1973) 791–797, http://dx.doi.org/10.1016/0001-6160(73)90043-6.
[10] L.E. Murr, G.I. Wong, R.J. Horylev, Measurement of interfacial free energies and associated temperature coefficients in 304 stainless steel, Acta Metall. 21 (5) (1973) 595–604, http://dx.doi.org/10.1016/0001-6160(73)90068-0.
[11] G.F. Bolling, On the average large-angle grain boundary, Acta Metall. 16 (9) (1968) 1147–1157, http://dx.doi.org/10.1016/0001-6160(68)90049-7.
[12] L. Missol, Orientation dependence of grain-boundarl energl in metals in the viel of a pseudoheterophase dislocation core model, Acta Metall. 24 (1) (1976) 73–79, http://dx.doi.org/10.1016/0001-6160(76)90149-8.
[13] M.C. Inman, H.R. Tipler, Interfacial energy and composition in metals and alloys, Metall. Rev. 8 (1) (1963) 105–166, http://dx.doi.org/10.1179/mtlr.1963.8.1.105.
[14] L. Bryant, R. Speiser, J. Hirth, Some interfacial properties of fcc cobalt, Trans. AIME 242 (1968) 1145.
[15] J.E. Hilliard, M. Cohen, B.L. Averbach, Grain-boundary energies in gold-copper alloys, Acta Metall. 8 (1) (1960) 26–31, http://dx.doi.org/10.1016/0001-6160(60)90136-X.
[16] E.D. Hondros, N.P. Allen, The influence of phosphorus in dilute solid solution on the absolute surface and grain boundary energies of iron, Proc. R. Soc. London. Ser. A. Math. Phys. Sci. 286 (1407) (1965) 479–498, http://dx.doi.org/10.1098/rspa.1965.0158.
[17] B.C. Allen, The surface free energy of solid molybdenum, J. Less Common Met. 17 (4) (1969) 403–410, http://dx.doi.org/10.1016/0022-5088(69)90066-6.
[18] E.N. Hodkin, M.G. Nicholas, D.M. Poole, The surface energies of solid molybdenum, niobium, tantalum and tungsten, J. Less Common Met. 20 (2) (1970) 93–103, http://dx.doi.org/10.1016/0022-5088(70)90093-7.
[19] B.C. Allen, The interfacial free energies of solid chromium, molybdenum and tungsten, J. Less Common Met. 29 (3) (1972) 263–282, http://dx.doi.org/10.1016/0022-5088(72)90114-2.
[20] T.A. Roth, The surface and grain boundary energies of iron, cobalt and nickel, Mater. Sci. Eng. 18 (2) (1975) 183–192, http://dx.doi.org/10.1016/0025-5416(75)90168-8.
[21] G.C. Hasson, C. Goux, Interfacial energies of tilt boundaries in aluminium. Experimental and theoretical determination, Scr. Metall. 5 (10) (1971) 889–894, http://dx.doi.org/10.1016/0036-9748(71)90064-0.
[22] H. Miura, M. Kato, T. Mori, Temperature dependence of the energy of Cu [110] symmetrical tilt grain boundaries, J. Mater. Sci. Lett. 13 (1) (1994) 46–48, http://dx.doi.org/10.1007/BF02352916.
[23] N.A. Gjostein, F.N. Rhines, Absolute interfacial energies of [001] tilt and twist grain boundaries in copper, Acta Metall. 7 (5) (1959) 319–330, http://dx.doi.org/10.1016/0001-6160(59)90198-1.
[24] W. Zhang, P. Sachenko, I. Gladwell, Thermal grain boundary grooving with anisotropic surface free energies, Acta Mater. 52 (1) (2004) 107–116, http://dx.doi.org/10.1016/j.actamat.2003.08.033.
[25] L. Klinger, E. Rabkin, Effects of surface anisotropy on grain boundary grooving, Interface Sci. 9 (2001) 55–63, http://dx.doi.org/10.1023/A:1011270830969.
[26] E. Rabkin, L. Klinger, V. Semenov, Grain boundary grooving at the singular surfaces, Acta Mater. 48 (7) (2000) 1533–1540, http://dx.doi.org/10.1016/S1359-6454(99)00432-2.
[27] E. Rabkin, L. Klinger, The fascination of grain boundary grooves, Adv. Eng. Mater. 3 (5) (2001) 277–282, http://dx.doi.org/10.1002/1527-2648(200105)3:5.
[28] J. Zimmerman, A. Aviv, Y. Elfassy, A. Bisht, L. Klinger, E. Rabkin, Thermal ridges – formation of hillock-like structures in deformed bulk nickel, Acta Mater. 237 (2022) 118151, http://dx.doi.org/10.1016/j.actamat.2022.118151.
[29] Y. Amouyal, E. Rabkin, A scanning force microscopy study of grain boundary energy in copper subjected to equal channel angular pressing, Acta Mater. 55 (20) (2007) 6681–6689, http://dx.doi.org/10.1016/j.actamat.2007.08.023.
[30] J. Zimmerman, A. Sharma, S. Divinski, E. Rabkin, Relative grain boundary energies in ultrafine grain Ni obtained by high pressure torsion, Scr. Mater. 182 (2020) 90–93, http://dx.doi.org/10.1016/j.scriptamat.2020.03.008.
[31] V.T. Borisov, V.M. Golikov, G.V. Scherbedinskiy, Relation between diffusion coefficients and grain boundary energy, Phys. Met. Metall. 17 (1964) 881–885.
[32] P. Guiraldenq, Diffusion intergranulaire et energie des joints de grains [grain boundary diffusion and energy], J. Phys. C. 36 (1975) 201–211, http://dx.doi.org/10.1051/jphyscol:1975420.
[33] D. Gupta, Grain-boundary energies and their interaction with Ta solute from self-diffusion in Au and Au-1·2 at. % Ta alloy, Phil. Mag. 33 (1) (1976) 189–197, http://dx.doi.org/10.1080/14786437608221103.
[34] D. Gärtner, L. Belkacemi, V.A. Esin, F. Jomard, A.A. Fedotov, J. Schell, J.V. Osinskaya, A.V. Pokoev, C. Duhamel, A. Paul, S.V. Divinski, Techniques of tracer diffusion measurements in metals, alloys and compounds, Diffus. Found. 29 (2021) 31–73, http://dx.doi.org/10.4028/www.scientific.net/DF.29.31.
[35] J. Pelleg, On the relation between diffusion coefficients and grain boundary energy, Phil. Mag. 14 (129) (1966) 595–601, http://dx.doi.org/10.1080/14786436608211954.
[36] D. Gupta, Influence of solute segregation on grain-boundary energy and self-diffusion, Metall. Trans. A 8 (9) (1977) 1431–1438, http://dx.doi.org/10.1007/BF02642856.
[37] P. Haremski, L. Epple, M. Wieler, P. Lupetin, R. Thelen, M.J. Hoffmann, A thermal grooving study of relative grain boundary energies of nickel in polycrystalline Ni and in a Ni/YSZ anode measured by atomic force microscopy, Acta Mater. 214 (2021) 116936, http://dx.doi.org/10.1016/j.actamat.2021.116936.
[38] S.V. Divinski, G. Reglitz, G. Wilde, Grain boundary self-diffusion in polycrystalline nickel of different purity levels, Acta Mater. 58 (2) (2010) 386–395, http://dx.doi.org/10.1016/j.actamat.2009.09.015.
[39] D. Prokoshkina, V.A. Esin, G. Wilde, S.V. Divinski, Grain boundary width, energy and self-diffusion in nickel: Effect of material purity, Acta Mater. 61 (14) (2013) 5188–5197, http://dx.doi.org/10.1016/j.actamat.2013.05.010.
[40] M. Glienke, M. Vaidya, K. Gururaj, L. Daum, B. Tas, L. Rogal, K. Pradeep, S.V. Divinski, G. Wilde, Grain boundary diffusion in CoCrFeMnNi high entropy alloy: Kinetic hints towards a phase decomposition, Acta Mater. 195 (2020) 304–316, http://dx.doi.org/10.1016/j.actamat.2020.05.009.
[41] E.A. Holm, D.L. Olmsted, S.M. Foiles, Comparing grain boundary energies in face-centered cubic metals: Al, Au, Cu and Ni, Scr. Mater. 63 (9) (2010) 905–908, http://dx.doi.org/10.1016/j.scriptamat.2010.06.040.
[42] D.L. Olmsted, S.M. Foiles, E.A. Holm, Survey of computed grain boundary properties in face-centered cubic metals: I. Grain boundary energy, Acta Mater. 57 (13) (2009) 3694–3703, http://dx.doi.org/10.1016/j.actamat.2009.04.007.
[43] S. Ratanaphan, D.L. Olmsted, V.V. Bulatov, E.A. Holm, A.D. Rollett, G.S. Rohrer, Grain boundary energies in body-centered cubic metals, Acta Mater. 88 (2015) 346–354, http://dx.doi.org/10.1016/j.actamat.2015.01.069.
[44] H. Zheng, X.G. Li, R. Tran, C. Chen, M. Horton, D. Winston, K.A. Persson, S.P. Ong, Grain boundary properties of elemental metals, Acta Mater. 186 (2020) 40–49, http://dx.doi.org/10.1016/j.actamat.2019.12.030.

[45] D. Scheiber, O. Renk, M. Popov, L. Romaner, Temperature dependence of surface and grain boundary energies from first principles, Phys. Rev. B 101 (17) (2020) 174103, http://dx.doi.org/10.1103/PhysRevB.101.174103.

[46] S.M. Foiles, Temperature dependence of grain boundary free energy and elastic constants, Scr. Mater. 62 (5) (2010) 231–234, http://dx.doi.org/10.1016/j.scriptamat.2009.11.003.

[47] T. Cheng, D. Fang, Y. Yang, The temperature dependence of grain boundary free energy of solids, J. Appl. Phys. 123 (8) (2018) http://dx.doi.org/10.1063/1.5017171.

[48] B. Runnels, A projection-based reformulation of the coincident site lattice Σ for arbitrary bicrystals at finite temperature, Acta Crystallogr. A 73 (2) (2017) 87–92, http://dx.doi.org/10.1107/S205327331700122X.

[49] B. Runnels, I.J. Beyerlein, S. Conti, M. Ortiz, An analytical model of interfacial energy based on a lattice-matching interatomic energy, J. Mech. Phys. Solids 89 (2016) 174–193, http://dx.doi.org/10.1016/j.jmps.2016.01.008.

[50] B. Runnels, I.J. Beyerlein, S. Conti, M. Ortiz, A relaxation method for the energy and morphology of grain boundaries and interfaces, J. Mech. Phys. Solids 94 (2016) 388–408, http://dx.doi.org/10.1016/j.jmps.2015.11.007.

[51] C. Wang, S. Schönecker, W. Li, Y. Yang, Q.M. Hu, L. Vitos, Twinning pathways in Fe and Fe–Cr alloys from first-principles theory, Acta Mater. 215 (2021) 117094, http://dx.doi.org/10.1016/j.actamat.2021.117094.

[52] M. De Jong, W. Chen, T. Angsten, A. Jain, R. Notestine, A. Gamst, M. Sluiter, C.K. Ande, S. Van Der Zwaag, J.J. Plata, et al., Charting the complete elastic properties of inorganic crystalline compounds, Sci. Data 2 (1) (2015) 1–13, http://dx.doi.org/10.1038/sdata.2015.9.

[53] W. Kohn, L.J. Sham, Self-consistent equations including exchange and correlation effects, Phys. Rev. 140 (1965) A1133–A1138, http://dx.doi.org/10.1103/PhysRev.140.A1133.

[54] P.E. Blöchl, Projector augmented-wave method, Phys. Rev. B 50 (1994) 17953–17979, http://dx.doi.org/10.1103/PhysRevB.50.17953.

[55] J.P. Perdew, A. Ruzsinszky, G.I. Csonka, O.A. Vydrov, G.E. Scuseria, L.A. Constantin, X. Zhou, K. Burke, Restoring the density-gradient expansion for exchange in solids and surfaces, Phys. Rev. Lett. 100 (13) (2008) 136406, http://dx.doi.org/10.1103/PhysRevLett.100.136406.

[56] D. Scheiber, R. Pippan, P. Puschnig, L. Romaner, Ab initiocalculations of grain boundaries in bcc metals, Modelling Simul. Mater. Sci. Eng. 24 (3) (2016) 35013, http://dx.doi.org/10.1088/0965-0393/24/3/035013.

[57] A. Patra, S. Jana, L.A. Constantin, L. Chiodo, P. Samal, Improved transition metal surface energies from a generalized gradient approximation developed for quasi two-dimensional systems, J. Chem. Phys. 152 (15) (2020) 151101, http://dx.doi.org/10.1063/1.5145367.

[58] C. Li, S. Lu, L. Vitos, Predicting grain boundary energies of complex alloys from ab initio calculations, Scr. Mater. 203 (2021) 114118, http://dx.doi.org/10.1016/j.scriptamat.2021.114118.

[59] J.Y. Lee, M. Punkkinen, S. Schönecker, Z. Nabi, K. Kádas, V. Zólyomi, Y. Koo, Q.-M. Hu, R. Ahuja, B. Johansson, J. Kollár, L. Vitos, S. Kwon, The surface energy and stress of metals, Surf. Sci. 674 (2018) 51–68, http://dx.doi.org/10.1016/j.susc.2018.03.008.

[60] B.J. Lee, M.I. Baskes, H. Kim, Y.K. Cho, Second nearest-neighbor modified embedded atom method potentials for bcc transition metals, Phys. Rev. B 64 (18) (2001) http://dx.doi.org/10.1103/PhysRevB.64.184102.

[61] W.R. Tyson, W.A. Miller, Surface free energies of solid metals: Estimation from liquid surface tension measurements, Surf. Sci. 62 (1) (1977) 267–276, http://dx.doi.org/10.1016/0039-6028(77)90442-3.

[62] B. Medasani, M. Haranczyk, A. Canning, M. Asta, Vacancy formation energies in metals: A comparison of metagga with LDA and GGA exchange-correlation functionals, Comput. Mater. Sci. 101 (2015) 96–107, http://dx.doi.org/10.1016/j.commatsci.2015.01.018.

[63] W. Hu, X. Shu, B. Zhang, Point-defect properties in body-centered cubic transition metals with analytic EAM interatomic potentials, Comput. Mater. Sci. 23 (1) (2002) 175–189, http://dx.doi.org/10.1016/S0927-0256(01)00238-5.

[64] C. Kittel, P. McEuen, P. McEuen, Introduction To Solid State Physics, Wiley New York, 1996.

[65] P. Villars, L.D. Calvert, Pearson's Handbook of Crystallographic Data for Intermediate Phases, American Society of Metals, Cleveland, OH, 1985.

[66] W. Setyawan, R.J. Kurtz, Ab initio study of H, He, Li and Be impurity effect in tungsten $\Sigma 3$ {112} and $\Sigma 27$ {552} grain boundaries, J. Phys.: Condens. Matter 26 (13) (2014) 135004, http://dx.doi.org/10.1088/0953-8984/26/13/135004.

[67] Y.A. Du, L. Ismer, J. Rogal, T. Hickel, J. Neugebauer, R. Drautz, First-principles study on the interaction of h interstitials with grain boundaries in α- and γ-Fe, Phys. Rev. B 84 (2011) 144121, http://dx.doi.org/10.1103/PhysRevB.84.144121.

[68] H. Udin, Grain boundary effect in surface tension measurement, Trans. AIME 3 (1) (1951) 63, http://dx.doi.org/10.1007/BF03398958.

[69] D.J. Rowenhorst, P.W. Voorhees, Measurements of the grain boundary energy and anisotropy in tin, Metall. Mater. Trans. A 36 (8) (2005) 2127–2135, http://dx.doi.org/10.1007/s11661-005-0333-7.

[70] B.C. Allen, Effect of rhenium on the interface energies of chromium, molybdenum, and tungsten, Trans. Met. Soc. AIME 236 (1966) http://dx.doi.org/osti.gov/biblio/4543708.

[71] M.A. Meyers, L.E. Murr, A model for the formation of annealing twins in FCC metals and alloys, Acta Metall. 26 (6) (1978) 951–962, http://dx.doi.org/10.1016/0001-6160(78)90046-9.

[72] T. Mori, H. Miura, T. Tokita, J. Haji, M. Kato, Determination of the energies of [001] twist boundaries in cu with the shape of boundary SiO2 particles, Phil. Mag. Lett. 58 (1) (1988) 11–15, http://dx.doi.org/10.1080/09500838808214724.

[73] A.D. Darbal, K.J. Ganesh, X. Liu, S.B. Lee, J. Ledonne, T. Sun, B. Yao, A.P. Warren, G.S. Rohrer, A.D. Rollett, et al., Grain boundary character distribution of nanocrystalline cu thin films using stereological analysis of transmission electron microscope orientation maps, Microsc. Microanal. 19 (1) (2013) 111–119, http://dx.doi.org/10.1017/S1431927612014055.

[74] V. Randle, G.S. Rohrer, H.M. Miller, M. Coleman, G.T. Owen, Five-parameter grain boundary distribution of commercially grain boundary engineered nickel and copper, Acta Mater. 56 (10) (2008) 2363–2373, http://dx.doi.org/10.1016/j.actamat.2008.01.039.

[75] D.M. Saylor, A. Morawiec, G.S. Rohrer, The relative free energies of grain boundaries in magnesia as a function of five macroscopic parameters, Acta Mater. 51 (13) (2003) 3675–3686, http://dx.doi.org/10.1016/S1359-6454(03)00182-4.

[76] G.S. Rohrer, J. Li, S. Lee, A.D. Rollett, M. Groeber, M.D. Uchic, Deriving grain boundary character distributions and relative grain boundary energies from three-dimensional EBSD data, Mater. Sci. Technol. 26 (6) (2010) 661–669, http://dx.doi.org/10.1179/026708309X12468927349370.

[77] J.L. Nilles, D.L. Olson, Energy of a bcc iron deformation twin boundary, J. Appl. Phys. 41 (2) (1970) 531–532, http://dx.doi.org/10.1063/1.1658707.

[78] T. Vystavel, J.M. Pénisson, A. Gemperle, High-resolution and conventional electron microscopy study of a Σ=3, [101]{121} twin grain boundary in molybdenum, Phil. Mag. A 81 (2) (2001) 417–429, http://dx.doi.org/10.1080/01418610108214312.

[79] P.D. Bristowe, A.G. Crocker, M.J. Norgett, The structure of twin boundaries in body centred cubic metals, J. Phys. F 4 (11) (1974) 1859–1864, http://dx.doi.org/10.1088/0305-4608/4/11/010.

[80] P.D. Bristowe, A.G. Crocker, A computer simulation study of the structures of twin boundaries in body-centred cubic crystals, Phil. Mag. 31 (3) (1975) 503–517, http://dx.doi.org/10.1080/14786437508226533.

[81] V.V. Bulatov, B.W. Reed, M. Kumar, Grain boundary energy function for fcc metals, Acta Mater. 65 (2014) 161–175, http://dx.doi.org/10.1016/j.actamat.2013.10.057.

[82] H. Beladi, G.S. Rohrer, The distribution of grain boundary planes in interstitial free steel, Metall. Mater. Trans. A 44 (1) (2013) 115–124, http://dx.doi.org/10.1007/s11661-012-1393-0.

[83] H. Beladi, N.T. Nuhfer, G.S. Rohrer, The five-parameter grain boundary character and energy distributions of a fully austenitic high-manganese steel using three dimensional data, Acta Mater. 70 (2014) 281–289, http://dx.doi.org/10.1016/j.actamat.2014.02.038.

[84] S. Divinski, J. Ribbe, G. Schmitz, C. Herzig, Grain boundary diffusion and segregation of Ni in Cu, Acta Mater. 55 (10) (2007) 3337–3346, http://dx.doi.org/10.1016/j.actamat.2007.01.032.

[85] A.D. Le Claire, The analysis of grain boundary diffusion measurements, Br. J. Appl. Phys. 14 (6) (1963) 351–356, http://dx.doi.org/10.1088/0508-3443/14/6/317.

[86] I. Herbeuval, M. Biscondi, C. Goux, Influence of intercrystalline structure on the diffusion of zinc in symmetrical bending boundaries of aluminum, Mem. Sci. Rev. Met. 70 (1) (1973) 39–46.

[87] R.W. Balluffi, R.F. Mehl Medalist, Grain boundary diffusion mechanisms in metals, Metall. Trans. A 13A (1982) 2069–2095, http://dx.doi.org/10.1007/BF02669167.

[88] A. Paul, T. Laurila, V. Vuorinen, S. Divinski, Thermodynamics, Diffusion and the Kirkendall Effect in Solids, Springer Int. Publ. Switzerland, 2014, http://dx.doi.org/10.1007/978-3-319-07461-0.

[89] Y.S. Kang, J.S. Lee, S.V. Divinski, C. Herzig, Ni grain boundary diffusion in coarse-grained Fe-40 wt.% Ni alloy and comparison with Ni diffusion in the nanocrystalline alloy, Int. J. Mater. Res. 95 (2) (2004) 76–79, http://dx.doi.org/10.3139/ijmr-2004-0018.

[90] D.I. Bolef, J.D. Klerk, Elastic constants of single-crystal Mo and W between 77° and 500° k, J. Appl. Phys. 33 (7) (1962) 2311–2314, http://dx.doi.org/10.1063/1.1728952.

[91] F.H. Featherston, J.R. Neighbours, Elastic constants of tantalum, tungsten, and molybdenum, Phys. Rev. 130 (4) (1963) 1324–1333, http://dx.doi.org/10.1103/PhysRev.130.1324.

[92] R. Lowrie, A.M. Gonas, Single-crystal elastic properties of tungsten from 24° to 1800°C, J. Appl. Phys. 38 (11) (1967) 4505–4509, http://dx.doi.org/10.1063/1.1709158.

[93] J.S. Lee, K. Klockgeter, C. Herzig, Grain boundary self and impurity diffusion in tungsten in the temperature range of activated sintering, J. Phys., Colloq. 51 (C1) (1990) C1–569, http://dx.doi.org/10.1051/jphyscol:1990189.

[94] J.L. Johnson, R.M. German, Theoretical modeling of densification during activated solid-state sintering, Metall. Mater. Trans. A 27 (2) (1996) 441–450, http://dx.doi.org/10.1007/BF02648421.

[95] J.S. Lee, C. Minkwitz, C. Herzig, Grain boundary self-diffusion in polycrystalline tungsten at low temperatures, Phys. Status Solidi b 202 (2) (1997) 931–940, http://dx.doi.org/10.1002/1521-3951(199708)202:2<931::AID-PSSB931>3.0.CO;2-O.

[96] Y. Hao, C. Tan, X. Yu, R. Chen, Z. Nie, Y. Ren, S. Yang, Y. Li, F. Wang, Effect of grain boundary misorientation angle on diffusion behavior in molybdenum-tungsten systems, J. Alloys Compd. 819 (2020) 152975, http://dx.doi.org/10.1016/j.jallcom.2019.152975.

[97] J. Lee, K. Vieregge, C. Herzig, The unusual temperature dependence of 57co grain boundary diffusion in tungsten: A contribution to the mechanism of activated sintering? Scr. Metall. 22 (10) (1988) 1639–1644, http://dx.doi.org/10.1016/S0036-9748(88)80257-6.

[98] X. Liu, D. Choi, H. Beladi, N.T. Nuhfer, G.S. Rohrer, K. Barmak, The five-parameter grain boundary character distribution of nanocrystalline tungsten, Scr. Mater. 69 (5) (2013) 413–416, http://dx.doi.org/10.1016/j.scriptamat.2013.05.046.

[99] S.V. Radcliffe, The surface energy of solid niobium, J. Less Common Met. 3 (5) (1961) 360–366, http://dx.doi.org/10.1016/0022-5088(61)90011-X.

[100] A.T. Price, H.A. Holl, A.P. Greenough, The surface energy and self diffusion coefficient of solid iron above 1350° C, Acta Metall. 12 (1) (1964) 49–58, http://dx.doi.org/10.1016/0001-6160(64)90053-7.

[101] D.W. James, G.M. Leak, Grain boundary diffusion of iron, cobalt and nickel in alpha-iron and of iron in gamma-iron, Phil. Mag. 12 (117) (1965) 491–503, http://dx.doi.org/10.1080/14786436508218895.

[102] J. Bernardini, P. Gas, E.D. Hondros, M.P. Seah, The role of solute segregation in grain boundary diffusion, Proc. R. Soc. London. Ser. A. Math. Phys. Sci. 379 (1776) (1982) 159–178, http://dx.doi.org/10.1098/rspa.1982.0011.

[103] H. Hänsel, L. Stratmann, H. Keller, H.J. Grabke, Effects of the grain boundary segregants P, S, C and N on the grain boundary self-diffusivity in alpha-iron, Acta Metall. 33 (4) (1985) 659–665, http://dx.doi.org/10.1016/0001-6160(85)90029-X.

[104] S.V. Divinski, J. Geise, E. Rabkin, C. Herzig, Grain boundary self-diffusion in α-iron of different purity: effect of dislocation enhanced diffusion, Z. Met.kd. 95 (10) (2004) 945–952, http://dx.doi.org/10.3139/146.018036.

[105] A. Inoue, H. Nitta, Y. Iijima, Grain boundary self-diffusion in high purity iron, Acta Mater. 55 (17) (2007) 5910–5916, http://dx.doi.org/10.1016/j.actamat.2007.06.041.

[106] E. Barbé, C.C. Fu, M. Sauzay, Fracture of coherent interfaces between an fcc metal matrix and the Cr23C6 carbide precipitate from first principles, Phys. Rev. Mater. 2 (2) (2018) 023605, http://dx.doi.org/10.1103/PhysRevMaterials.2.023605.

[107] Z.S. Basinski, A.L. Sutton, The lattice expansion of iron, Proc. R. Soc. London. A 229 (1955) 459–467, http://dx.doi.org/10.1098/rspa.1955.0102.

[108] J. Zarestky, C. Stassis, Lattice dynamics of γ-Fe, Phys. Lett. A 35 (9) (1987) 4500–4502, http://dx.doi.org/10.1103/PhysRevB.35.4500.

[109] J. Neuhaus, M. Leitner, K. Nicolaus, W. Petry, B. Hennion, A. Hiess, Role of vibrational entropy in the stabilization of the high-temperature phases of iron, Phys. Rev. B 89 (184302) (2014) 1–6, http://dx.doi.org/10.1103/PhysRevB.89.184302.

[110] Q. Li, D.H. Huang, Q.L. Cao, F.H. Wang, L.C. Cai, X.L. Zhang, F.Q. Jing, Thermodynamics and elastic properties of ta from first-principles calculations, Chin. Phys. B 21 (12) (2012) http://dx.doi.org/10.1088/1674-1056/21/12/127102.

[111] D. Dragoni, D. Ceresoli, N. Marzari, Thermoelastic properties of α -iron from first-principles, Phys. Rev. B 91 (10) (2015) 1–11, http://dx.doi.org/10.1103/PhysRevB.91.104105.

[112] E. Walker, Anomalous temperature behaviour of the shear elastic constant C44 in vanadium, Solid State Commun. 28 (1978) 587–589, http://dx.doi.org/10.1016/0038-1098(78)90495-7.

[113] Y. Talmor, E. Walker, S. Steinemann, Elastic constants of nionium up to the melting point, Solid State Commun. 23 (9) (1977) 649–651, http://dx.doi.org/10.1016/0038-1098(77)90541-5.

[114] E. Walker, P. Bujard, Anomalous temperature behaviour of the shear elastic constant C44 in tantalum, Solid State Commun. 34 (8) (1980) 691–693, http://dx.doi.org/10.1016/0038-1098(80)90957-6.

[115] P. Bujard, R. Sanjines, E. Walker, J. Ashkenazi, M. Peter, Elastic constants in Nb-Mo alloys from zero temperature to the melting point: Experiment and theory, J. Phys. F Met. Phys. 11 (4) (1981) 775–786, http://dx.doi.org/10.1088/0305-4608/11/4/011.

[116] L. Huang, M. Ramzan, L. Vitos, B. Johansson, R. Ahuja, Anomalous temperature dependence of elastic constant c44 in V, Nb, Ta, Pd, and Pt, J. Phys. Chem. Solids 71 (8) (2010) 1065–1068, http://dx.doi.org/10.1016/j.jpcs.2010.03.007.

[117] P. Keuter, D. Music, V. Schnabel, M. Stuer, J.M. Schneider, From qualitative to quantitative description of the anomalous thermoelastic behavior of V, Nb, Ta, Pd and Pt, J. Phys.: Condens. Matter 31 (22) (2019) 225402, http://dx.doi.org/10.1088/1361-648X/ab099b.

[118] J.T. Smith, Diffusion mechanism for the nickel-activated sintering of molybdenum, J. Appl. Phys. 36 (2) (1965) 595–598, http://dx.doi.org/10.1063/1.1714036.

[119] S. Majumdar, S. Raveendra, I. Samajdar, P. Bhargava, I.G. Sharma, Densification and grain growth during isothermal sintering of Mo and mechanically alloyed Mo–TZM, Acta Mater. 57 (14) (2009) 4158–4168, http://dx.doi.org/10.1016/j.actamat.2009.05.013.

[120] M.P. Punkkinen, S.K. Kwon, J. Kollár, B. Johansson, L. Vitos, Compressive surface stress in magnetic transition metals, Phys. Rev. Lett. 106 (5) (2011) 23–26, http://dx.doi.org/10.1103/PhysRevLett.106.057202.

[121] R. Singh, J.H. Schneibel, S. Divinski, G. Wilde, Grain boundary diffusion of fe in ultrafine-grained nanocluster- strengthened ferritic steel, Acta Mater. 59 (4) (2011) 1346–1353, http://dx.doi.org/10.1016/j.actamat.2010.10.067.

[122] H. Schmidt, S. Chakravarty, M. Jiang, E. Hüger, P.K. Parida, T. Geue, J. Stahn, U. Tietze, D. Lott, Grain boundary self-diffusion in fe films with a stable nanostructure, J. Mater. Sci. 47 (9) (2012) 4087–4092, http://dx.doi.org/10.1007/s10853-012-6262-0.

[123] G. Stechauner, E. Kozeschnik, Assessment of substitutional self-diffusion along short-circuit paths in Al, Fe and Ni, CALPHAD 47 (2014) 92–99, http://dx.doi.org/10.1016/j.calphad.2014.06.008.

[124] S. Starikov, M. Mrovec, R. Drautz, Study of grain boundary self-diffusion in iron with different atomistic models, Acta Mater. 188 (2020) 560–569, http://dx.doi.org/10.1016/j.actamat.2020.02.027.

[125] T. Surholt, C. Herzig, Grain boundary self-diffusion in cu polycrystals of different purity, Acta Mater. 45 (9) (1997) 3817–3823, http://dx.doi.org/10.1016/S1359-6454(97)00037-2.

[126] S.V. Divinski, B.S. Bokstein, Recent advances and unsolved problems of grain boundary diffusion, Defect Diffus. Forum 309–310 (2011) 1–8, http://dx.doi.org/10.4028/www.scientific.net/DDF.309-310.1.

[127] S. Baroni, S. de Gironcoli, A. Dal Corso, P. Giannozzi, Phonons and related crystal properties from density-functional perturbation theory, Rev. Modern Phys. 73 (2) (2001) 515–562, http://dx.doi.org/10.1103/RevModPhys.73.515.

[128] S.L. Shang, Y. Wang, D. Kim, Z.-K. Liu, First-principles thermodynamics from phonon and debye model: Application to Ni and Ni3Al, Comput. Mater. Sci. 47 (4) (2010) 1040–1048, http://dx.doi.org/10.1016/j.commatsci.2009.12.006.

[129] S.A. Etesami, E. Asadi, Molecular dynamics for near melting temperatures simulations of metals using modified embedded-atom method, J. Phys. Chem. Solids 112 (2018) 61–72, http://dx.doi.org/10.1016/j.jpcs.2017.09.001.

[130] X. Li, S. Schönecker, X. Li, J. Zhao, L. Vitos, The influence of temperature on the elastic properties of body-centered cubic reduced activation steels, Mater. Des. 197 (2021) 109282, http://dx.doi.org/10.1016/j.matdes.2020.109282.

[131] S. Schönecker, S.K. Kwon, B. Johansson, L. Vitos, Surface parameters of ferritic iron-rich fe-cr alloy, J. Phys.: Condens. Matter 25 (30) (2013) http://dx.doi.org/10.1088/0953-8984/25/30/305002.

[132] Y. Yamazaki, M. Sugihara, S. Takaki, K. Abiko, Y. Iijima, Volume and grain-boundary self-diffusion in a high-purity Fe-50 mass% Cr alloy, Phys. Status Solidi A 189 (1) (2002) 97–105, http://dx.doi.org/10.1002/1521-396X(200201)189.

[133] J. Čermák, J. Růžičková, A. Pokorná, Low-temperature tracer diffusion of chromium in Fe - Cr ferritic alloys, Scr. Mater. 35 (3) (1996) 411–416, http://dx.doi.org/10.1016/1359-6462(96)00148-0.

[134] Y. Shibuta, S. Takamoto, T. Suzuki, Dependence of the grain boundary energy on the alloy composition in the bcc iron-chromium alloy: A molecular dynamics study, Comput. Mater. Sci. 44 (4) (2009) 1025–1029, http://dx.doi.org/10.1016/j.commatsci.2008.07.013.